Chapter

Modeling Radiation Damage in Materials Relevant for Exploration and Settlement on the Moon

Natalia E. Koval, Bin Gu, Daniel Muñoz-Santiburcio and Fabiana Da Pieve

Abstract

Understanding the effect of radiation on materials is fundamental for space exploration. Energetic charged particles impacting materials create electronic excitations, atomic displacements, and nuclear fragmentation. Monte Carlo particle transport simulations are the most common approach for modeling radiation damage in materials. However, radiation damage is a multiscale problem, both in time and in length, an aspect treated by the Monte Carlo simulations only to a limited extent. In this chapter, after introducing the Monte Carlo particle transport method, we present a multiscale approach to study different stages of radiation damage which allows for the synergy between the electronic and nuclear effects induced in materials. We focus on cumulative displacement effects induced by radiation below the regime of hadronic interactions. We then discuss selected studies of radiation damage in materials of importance and potential use for the exploration and settlement on the Moon, ranging from semiconductors to alloys and from polymers to the natural regolith. Additionally, we overview some of the novel materials with outstanding properties, such as low weight, increased radiation resistance, and self-healing capabilities with a potential to reduce mission costs and improve prospects for extended human exploration of extraterrestrial bodies.

Keywords: space radiation, multiscale modeling, defects, semiconductors, alloys, composites, solar cells, habitat on the Moon

1. Introduction

Preparing for life on another planet or a planetary object requires an enormous effort from scientists and engineers [1]. The first steps toward extraterrestrial life are the crewed missions to the Moon, aiming to build the basis for the future long-term presence of humans beyond Earth. A remarkable amount of research and feasibility studies are being done by the European Space Agency (ESA) in Europe [2] and the National Aeronautics and Space Administration (NASA) in the USA [3, 4] on how to construct a

"new home in space," in a manner to eliminate the need for supply materials from Earth.

In this context, the use of space resources is one of the key directions in preparation for future human missions to the Moon. The so-called *in situ* Resource Utilization (ISRU) program by ESA and NASA explores the possibility of converting local resources of space bodies into valuable products and materials [5–8]. ISRU will ensure the sustainability and energy efficiency of space exploration, reduce the cost of delivery from Earth, and minimize mission risks. Among the topics of current ISRU research are producing metals and construction materials by transforming local regolith and rocks [9, 10], harvesting oxygen and hydrogen from minerals and water [10, 11], and growing plants [12, 13]. In this sense, the development of structurally sound composite materials with superior properties that can benefit from ISRU is crucial for preparing missions to the Moon. Many aspects of habitat construction, from large-scale infrastructure (e.g., communication and energy generation and storage) to manufacturing (e.g., equipment, tools, and machinery), would benefit from ISRU.

In space and on the lunar surface, there are many factors potentially leading to damage in materials, such as exposure to vacuum, extreme thermal conditions, impact collisions with micrometeoroids, and radiation [14]. Among these, radiation is considered particularly harmful for different functional components and instruments of spacecraft and lunar surface missions. Radiation can induce structural defects that evolve from nanoscale to micro- and macro-damage, causing degradation of the mechanical, thermal, and electrical properties of materials or can even lead to direct failure in electronic signals before interacting with the very structural composition of the material. Therefore, improving the radiation resistance of materials to be used in space missions and searching for more radiation-resistant materials is of utmost importance. The research effort is directed toward finding composite materials that can better withstand radiation and other challenges faced by mission components in space and on space bodies and exhibit self-healing capabilities [15].

In this chapter, we first introduce some relevant materials for two of the most critical applications on the Moon, i.e., habitat construction and energy production. Then, we provide an overview of the radiation environment on the lunar surface and different radiation effects that can be induced in materials by such an environment. We then discuss the ways of combining traditional methods commonly used to study radiation effects with recent advanced approaches in materials modeling and provide examples of radiation-effects modeling studies on different materials. Additionally, we discuss the possibilities of using novel promising materials with exceptional properties relevant for space exploration, with an emphasis on their radiation resistance.

2. Materials for practical applications on the Moon

NASA has identified the most important components of the lunar mission as (i) design and construction of habitats and (ii) resource and power management [16]. In particular, the emphasis is on lightweight materials that will be critical for mass reduction and thus increase the science return of the mission. Both components mentioned above will strongly rely on ISRU, i.e., *in situ* regolith processing and recycling [8, 17]. Below we provide examples of materials that will be of use for both habitat construction and power generation.

2.1 Materials for habitats

Constructing a habitat on the Moon can be done in two ways, by delivering materials from Earth and by using local resources. Although the latter option is more sustainable, the first one cannot be completely avoided. An important consideration that needs to be made when choosing materials is the type of habitat. NASA considers several types of habitat for different use, namely rigid (metals, alloys, and concrete) [18], inflatable (e.g., inflatable concrete [19]), or hybrid structures, as well as underground construction [20]. Depending on the type of habitat, different materials will be used [16, 21]. For example, unprocessed lunar regolith may be used for radiation shielding of habitat (e.g., lunar regolith geopolymer) [22–25], as well as for construction when converted into concrete [26, 27], 3D-printed [28–30], or processed into other construction material (e.g., bricks and glass) [16, 21]. For materials delivered from Earth, it is crucial to ensure their low weight, as well as resistance to very high and very low temperatures (which change from 127°C in the daytime to −173°C at night on the Moon surface) and radiation, durability, reusability, and structural reliability [16].

Metals and alloys are essential structural materials for construction given their compressive strength and good tensile properties and for other applications, such as energy carrier/storage (wires) [31] or equipment (e.g., excavation tools, molds, and rovers) [32]. Al, Ca, Fe, Ti, and Mg are the most abundant metals in the lunar regolith, which also contains smaller amounts of Ni, Cr, Mn, Zr, and V [5, 20]. These metals—together with Si, also abundant on the Moon—can be used to produce alloys. However, only Fe can be easily separated from regolith (using magnets). Other metals are present in the form of oxides and thus have to be obtained by manufacturing. Metal and alloy manufacturing will be extremely important for the exploration of the Moon as they represent an essential part of the construction and are critical ingredients for most technologies.

2.2 Materials for energy production

One of the crucial steps toward the Moon exploration and settlement is a reliable energy technology for electricity generation and power storage [33, 34] that would withstand the temperature gradients, high levels of radiation, and impact. The primary energy sources considered for future crewed lunar missions are solar power [35, 36], nuclear power [37], and fuel cells [38, 39]. Other ways may include the production of electricity from the excess heat from the sunlight collected by an "evergreen" inflatable dome [40]. In this chapter, we focus on solar cells, a safe and reliable source of electricity in space.

In the past decades, solar cells for space applications have evolved from single-crystalline Si-based cells to multi-junction (MJ) ones based on GaInP, GaAs, and Ge [41–43]. A promising class of materials for next-generation lightweight and high-power-conversion efficiency [44] solar cells are hybrid organic-inorganic perovskites (HOIPs) [45–47], which are considered as potential candidates for use on future lunar bases [34].

HOIPs possess a unique combination of properties, such as enhanced charge carrier mobility [48–51], diffusion length, and lifetime [48, 52, 53], high optical absorption [54, 55], and low production costs [56], representing a paradigm shift in solar cell technology [57] on Earth [58] and for space applications [59–62]. Given their flexibility [63], low weight, small dimensions (0.5 μm as compared to 200 μm for Si solar cells), the possibility of *in situ* manufacturing via 3D-printing techniques

[60, 64, 65] at low temperature, and their high resistance to radiation [60, 66–71], HOIPs qualify as exceptional candidates for easily deployable and resilient solar cells in space missions.

3. Radiation environment on the Moon and its effect on materials

3.1 Radiation environment on the lunar surface

The radiation environment on the Moon is constituted, apart from solar electromagnetic radiation, by three radiation "populations"—the constant solar wind, the intense but sporadic Solar Energetic Particles (SEPs), and the constant background of Galactic Cosmic Rays (GCRs). A summary of the radiation environment on the lunar surface is given in **Table 1**.

The solar wind is a constant flux of plasma from the upper atmosphere of the Sun. It consists mainly of ionized hydrogen (protons and electrons), a small percentage of α-particles, and trace amounts of heavier ions, with kinetic energy between 0.5 and 2 keV/nucleon [75]. The solar wind flux, temperature, density, and speed vary over time and solar longitude and latitude. The lunar surface is under continuous bombardment by the solar wind, as the Moon does not have a significant global geomagnetic field that could deflect solar particles. Particles penetrate the surface and undergo collisions with the ions of the lunar regolith. Their penetration depth depends on the impact energy, angle of incidence, and composition of the target surface. For a proton with a nominal energy of 1 keV, the penetration depth is typically about 20 nm [79]. The implanted protons diffuse and chemically combine with the regolith atoms, such as oxygen, or become trapped in physical defects. Recent studies have suggested that the implantation of solar wind protons in the lunar regolith is a major source of hydrogen in the formation of OH/H_2O [80, 81], whose presence is confirmed by experimental measurements [82].

SEPs originate from solar transient events, such as coronal mass ejections or flares, and consist in a sudden intense flux of high-energy protons and electrons (and a small amount of α-particles and heavier ions) [76, 78]. Typical energies of SEPs range from ten to hundreds of MeV. Such transient events have a higher occurrence probability during solar maximum, but they may also occur during solar minimum. Studies have shown that the lunar surface can charge to a high negative potential up to a few kV during SEP events [83, 84]. Such values of the potentials are much higher than the typical night-side potentials of a few hundred volts negative and may increase the risk of electrostatic discharge. The latter represents an additional hazard to the already dangerous radiation environment on the lunar surface.

GCRs constitute the slowly varying, low-intensity (few particles/cm^2(m^2) per second), highly-energetic radiation background in space. They are mainly

Source	Particles	Energy, MeV/nuc	Flux, nuc/cm^2/s
Solar Wind	Protons & electrons ~95%, α-particles ~4%, heavy ions ~1%	$\sim 10^{-3}$	$\sim 10^{8}$
SEPs	Protons >90%, electrons, α-particles, heavy ions <1%	~1–10^2	0 – 10^6
GCRs	Protons ~ 87%, α-particles ~12%, heavy ions ~1%	~10^2–10^4	2–4

Table 1.
Radiation particle types, their flux, and energies on the lunar surface [72–78].

associated with supernova explosions in the galaxy, but extra-galactic contributions also exist. GCRs are constituted by ~87% of hydrogen ions (protons), 12% of α-particles, 1–2% of high-energy and highly charged ions (high-charge Z and energy (HZE)-particles), and 1% of electrons and positrons [85]. The energy spectrum of GCRs covers a wide range, extending roughly up to 10^{18} eV, with higher energies (up to 10^{21} eV) being associated with ultrahigh-energy GCRs originating from extra-galactic sources. GCRs are modulated by the heliospheric field linked to solar activity. At solar maximum, the solar magnetic field increases, shielding the heliosphere from the lowest energy component of GCRs [86], thus decreasing the overall GCRs flux. At the solar minimum, the reduced solar magnetic field leads to a more intense GCRs flux in our interplanetary space [87, 88].

The annual exposure caused by GCRs on the lunar surface is ~380 mSv during solar minimum and ~110 mSv during solar maximum, as compared to the annual dose of natural ionizing radiation of 2.4 mSv on Earth [89] (1 Sv—1 Sievert, represents the equivalent biological effect of the deposit of a Joule of radiation energy in a kilogram of human tissue). The worst-case scenario studies suggest that SEPs may lead to a much higher exposure of ~1 Sv or even reach >2 Sv per event [90]. Studies of the radiation dose of GCRs and SEPs at the lunar surface and in a lava tube [90, 91] have shown that the exposure may be reduced to values similar to Earth in horizontal lava tubes.

3.2 Radiation-induced effects in materials

The effects of radiation on materials and devices can be cumulative (long term) and noncumulative (caused even by a single particle). The so-called Single Event Effects (SEEs) can occur when an ionizing particle passing through an electronic device carries a charge large enough to affect the device's performance. SEEs in aerospace technology can lead to errors, corrupt the data, create noise, reset the device, or even cause fatal part failure [92–95]. Cumulative radiation damage, on the other hand, occurs through continuous radiation exposure or exposure to intense flux due to SEPs events and can lead to the degradation of optical components and solar cells, eventually causing permanent damage. The total ionizing dose experienced by an electronic device can cause variations in threshold voltage or leakage current.

Cumulative non-ionizing damage in materials due to protons, electrons, and neutrons (originating from the interaction of energetic protons and electrons with the lunar surface) leads to defect formation (displacement damage) [94]. The types and sources of radiation, as well as the effects it can cause in materials, are summarized in **Table 2**.

Particle type	Energy	Sources	Radiation effects
Electrons	>1 MeV	SEPs	Ionization radiation damage
Protons	$0.1-1$ MeV	SEPs	Surface damage to materials
Protons	$1-10$ MeV	SEPs accelerated in shocks	Displacement damage in solar cells
Protons	>10 MeV	SEPs and GCRs	Ionization and displacement damage, background counting in sensors
Protons	>50 MeV	SEPs and GCRs	Single event effects
Ions	>10 MeV/nuc	SEPs and GCRs	Single event effects

Table 2.
Sources and types of radiation and the effects it causes in materials and devices [96].

Cumulative radiation damage is a multiscale process in terms of time and length. A schematic representation of the so-called displacement damage cascade is shown in **Figure 1**. At first, an energetic external particle approaches (**Figure 1**(1)) and enters the target (**Figure 1**(2)). As the particle passes through the material, it first transfers its kinetic energy to electronic degrees of freedom of the target (electronic stopping) (**Figure 1**(3)). Electronic excitations happen at a very short time scale (~100 as). After the particle has been slowed down by the target's electrons, it undergoes nuclear elastic collisions, displacing atoms in the target (Primary Knock-on Atoms, PKAs) that constitute themselves additional projectiles (**Figure 1**(4)). The PKA collides with other atoms creating a cascade of collisions [97] (**Figure 1**(5)). Atomic displacements induce the creation of different types of point defects, such as vacancies and interstitials (Frenkel pairs) and defect clusters (**Figure 1**(6)) and happen on a much longer time scale (up to ns). Eventually, many defects are healed due to the thermal motion of atoms (annealing stage, **Figure 1**(7)), leaving a finite number of defects in the structure (**Figure 1**(8)).

Atomic displacements described above lead to defect clustering and eventual amorphization in crystalline materials. Consequently, mechanical, physical, and other properties of the irradiated material can be significantly altered. The scale of the changes depends on the energy of incoming particles and the actual number and spatial distribution of survived defects after eventual self-healing [98].

The radiation-induced effects after atomic displacements strongly depend on the type of material. For metals and metallic alloys, the main effect of radiation is the generation of dislocation loops and point defects which cause significant radiation-induced strengthening or hardening. As a result, the ductility and fracture toughness of the metals (alloys) can be reduced, leading to brittle behavior [99]. Ductile-to-brittle transition is especially pronounced at low temperatures at which the defect mobility, and consequently the annealing of defects, is reduced.

As to other materials, such as semiconductors in solar cells, cumulative exposure to space radiation or high SEPs fluxes can strongly affect the performance of MJ solar cells [100]. Moreover, the impacting radiation can reduce the transmittance of the protective SiO_2 cover-glass on top of MJ cells by inducing color centers in the oxide material. The color centers appear when electrons excited by radiation become trapped by impurities in the oxide to form stable defect complexes. On the other hand, the radiation which is not blocked by the cover-glass causes damage in the functional layers of MJ solar cells by displacing atoms. Different energy levels can be created within the bandgap as a consequence of such structural defects. Such

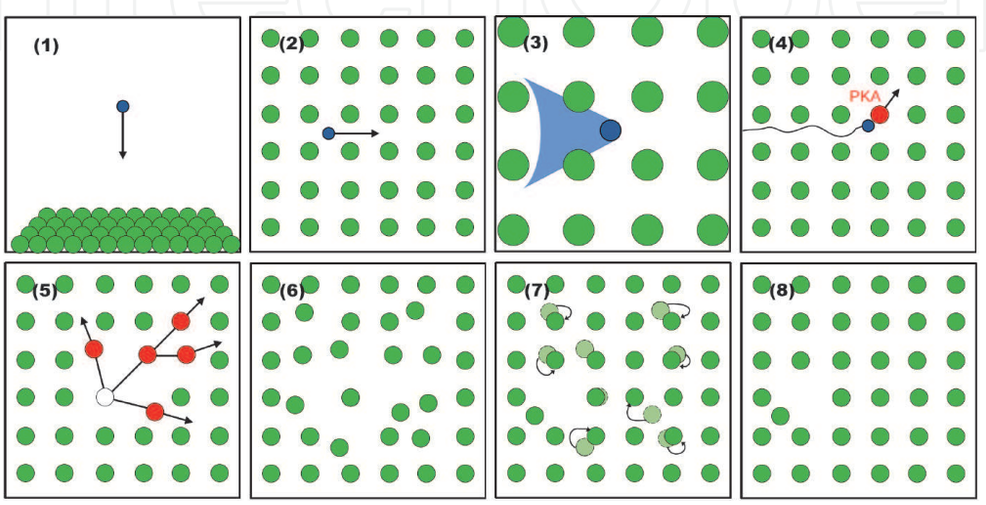

Figure 1.
Schematic representation of different stages of the damage cascade in a crystalline material under irradiation.

electronic defect levels affect the electrical performance of MJ solar cells acting as traps, recombination centers, or carrier removal sites which reduce free carrier concentration [100, 101].

Below, we will present different methods used to describe radiation-induced effects in materials focusing on the description of cumulative effects related to atomic displacements.

4. Monte Carlo particle transport modeling of radiation effects in materials

High-energy charged particles undergo a daunting number of interactions with target materials. Such interactions include:

i. electronic collisions leading to ionization and excitation;

ii. multiple Coulomb scattering at small angles (elastic deflection without energy loss, or minimal inelastic loss);

iii. inelastic nuclear reactions, that is, high-energy reactions in which a nucleus in the target struck by an incident particle (with energy >10 MeV) undergoes fragmentation into secondary lighter nuclei and other lighter particles;

iv. elastic nuclear interactions (<10–20 MeV) in which atoms are displaced from their initial positions creating point defects.

The most commonly used approach to study radiation-induced effects in materials is the Monte Carlo (MC) particle transport method [102, 103]. In MC particle transport, the interactions of individual primary ions and their secondaries are sampled to build a history of charged particle passage and energy deposition in the target [104], with a large enough statistical sample of trajectories. The energy- and angle-dependent cross sections for different interactions are provided by theoretical models of the elementary interactions and/or experimental data, depending on the energy window. Codes, such as Geant4 [105], MCNP6 [106–108], FLUKA [109], PHITS [110], and HETC-HEDS [111], have been successfully applied to study the radiation at a hemispherical dome made of lunar regolith used to simulate a lunar habitat [112, 113] and the radiation environment around the Moon [114, 115].

Several relevant radiation-induced effects in materials are due to particles with an energy of a few MeV to a few tenths of MeV, as can be seen in **Table 2**. In this regime, below hadronic interactions causing fragmentation/spallation, atomic displacements are induced in the target by elastic nuclear interactions. Two concepts describe the slowing down of the impacting particles (and the induced secondaries), (i) the *electronic stopping power*, that is, the energy loss of the moving particle to the electronic degrees of freedom of the target (a concept valid in the whole energy range) and (ii) the *nuclear stopping power*, that is, the energy lost to elastic nuclear interactions causing atomic displacements (a concept only used for the regime below hadronic interactions). MC particle transport modeling is a very convenient approach to deal with the enormous amount of interactions that a high-energy particle can induce in a target. However, the approximations used for intermediate and low energies (few MeV and lower) may pose some challenges for the applicability of MC particle transport. At such energies, the atomic-scale structure and the electronic properties of the target system should be taken into account for a

reliable description of the radiation-induced effects. In MC particle transport, however, the target materials are amorphous and the macroscopic interaction cross sections, as well as electronic and nuclear stopping power, are obtained by a simple stoichiometric averaging of the elemental cross sections and stopping power. The electronic stopping in MC particle transport simulations is calculated for a uniform electron gas with the same density as the target within the perturbative linear approach not appropriate at low energies [116]. Since the crystal structure of the target is ignored, the effects due to ion channeling (i.e., when the ion path is confined within the crystallographic planes), that have been shown to significantly influence the electronic stopping power [117, 118], are not taken into account.

A displacement cascade in MC particle transport simulations is generally modeled within the Binary Collision Approximation (BCA) [119] which assumes a series of independent two-body collisions. Between collisions, particles travel in a straight line. The BCA is valid when (i) the projectile energy is higher than 1 keV per nucleon, which, for PKAs, could be relevant energy, and (ii) the target material has low density, in which case the collisions between the incoming particle and the target atoms occur rarely. BCA allows reducing the computational complexity of the ion-matter interactions compared to a full many-body simulation (e.g., molecular dynamics, discussed in Section 5) and allows for reaching large dimensions with reduced computational needs. However, this method is valid for linear collisions only and describes only primary damage, that is, it does not account for the dynamic evolution of induced defects at later times (**Figure 2**).

One of the most popular tools in which the BCA is implemented is the Stopping and Range of Ions in Matter (SRIM) code [120]. Besides containing semiempirical data for the electronic stopping power of a variety of targets, SRIM can be applied to model the linear cascades and estimate the number of defects in any material and any ion energy up to 1 GeV. Nuclear stopping in very low-energy intervals uses the so-called ZBL (Ziegler-Biersack-Littmark) universal potential that combines classical Coulomb potential with a semiempirical screening function [120]. The electronic and nuclear degrees of freedom are completely separated in SRIM as well as in other MC particle transport tools used by the particle physics community and the space radiation effects community. Finally, it is important to remark that materials are static in MC particle transport methods—there is no dynamics induced in them by the impact of primaries and the generation and passage of secondaries. Thus, more accurate methods are needed to get access to the processes missing in MC particle transport calculations. Such methods are described in the next section.

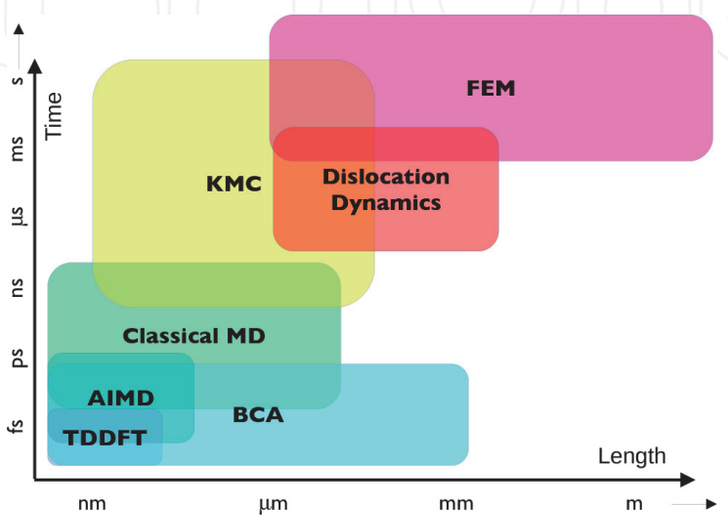

Figure 2.
Time and length scales and corresponding methods can be applied to study different stages of radiation damage.

5. Multiscale approach to modeling radiation damage in materials

There is a large variety of methods used in condensed matter physics and materials science to study radiation effects in materials, each of them describing a particular aspect of the damage process. **Figure 2** shows a schematic representation of the different time and length scales with the corresponding computational methods that can be applied to study different stages of radiation damage [97, 121, 122]. The very first stage, at the smallest time-length scale, is the electronic stopping regime. For decades, the semiempirical SRIM code discussed in the previous section has been the most widely used tool to calculate electronic stopping power. Nowadays, the electronic stopping power (and the induced electronic excitations in the target) can be described by *ab initio* (parameter-free) methods relying on a realistic description of the electronic and ionic properties of the target system. One of the most accurate methods for treating electronic excitations in materials is time-dependent density functional theory (TDDFT) [123] which allows accessing the electronic effects accompanying the ion dynamics. *Ab initio* molecular dynamics (AIMD) [124] based on density functional theory (DFT) [125, 126] can be applied to study point defect formation. At longer time scales and larger length scales, when atomic displacements start to dominate, classical molecular dynamics (MD) and the BCA are usually applied to perform collision cascade simulations. The kinetic Monte Carlo (KMC) [127], the dislocation dynamics (DD) [128], and the finite element method (FEM) [129] are used to study the evolution of defects at the even longer time and larger length scales.

For a complete and accurate description of every aspect of radiation damage, as well as the interplay between them, one has to adopt a combined approach. In recent years, researchers have realized the importance of a multiscale approach to studying radiation damage, as follows from many publications and reviews [121, 122, 130–134]. Each of the methods presented in **Figure 2**, as well the ways of combining them, will be discussed below in the order of increasing complexity. The main focus will be on classical MD, AIMD, and TDDFT, which are fundamental for the description of primary radiation damage at the atomic scale.

5.1 Classical molecular dynamics and beyond: the collision cascade

The most widely used approach in materials science to study the interaction of ions with matter (collision cascades) is MD [135]. MD offers a picture of the ion–ion interaction beyond the linear cascade of the pure BCA by including many-body effects. In MD, atoms are treated as classical particles, and their motion is described by Newtonian dynamics. No electronic effects are thus included.

Cascade simulations need large samples consisting of up to a million atoms (depending on the PKA's energy), which prohibits using parameter-free methods (such as DFT, see Section 5.2) to compute the interatomic forces. Instead, in MD, the forces on atoms are calculated from empirical or semiempirical interatomic potentials (also called force fields) [136–138]. MD with empirical potentials proved to work well for large systems and long time scales [139].

In an MD cascade simulation, the system is usually modeled using periodic boundary conditions, that is, by replicating a small unit cell in all directions. Typically, prior to the cascade simulation itself, a regular MD simulation is done to thermally equilibrate the target system at the desired initial temperature. Then, with the equilibrated configuration, the cascade simulation is initiated by changing the velocity of one of the atoms (the PKA), giving it the desired amount of kinetic energy in the intended direction. The system is then evolved in time as in regular MD, that is, by integrating Newton's equations along with a series of time-steps,

which involves computing the atomic forces, velocities, and positions at each time-step (see Refs. [140, 141] for classical texts on MD). At the end of the cascade simulation, the number of defects is obtained by evaluating the final geometry of the system. Usually, cascade simulations are repeated several times, choosing a different PKA and/or a different direction of the PKA's movement to obtain a statistical average of the number of final defects.

MD has been successfully applied to simulate radiation cascades in a variety of materials [139], from simple metals [142, 143] and compounds [144–146] to complex nanostructures [147], 2D materials [148], and novel multicomponent alloys [149, 150]. MD simulations can afford to access the processes taking place on a relatively long time scale up to ps or even ns which is enough to describe the damage cascade until the thermal spike of the collision has dissipated. Most of the MD codes, however, describe only elastic collisions between atoms and disregard the energy loss mechanisms such as electronic excitation and ionization. The possibility of including electronic excitations is discussed in Section 5.3.

After the primary damage has been formed, defects may continue diffusing, thus annihilating or forming defect clusters. Such processes occur on a much longer time scale, reaching at least seconds, not accessible via regular MD. The problem of simulating a process not accessible in a feasible amount of computational time has motivated the development of several enhanced sampling techniques [151], which in the case of MD simulations of materials have allowed to observe otherwise challenging processes, such as phase transitions.

KMC [127] simulations are commonly used to access long-time effects of radiation in materials [152–155]. KMC is designed to model the time evolution of an atomic system. However, instead of solving the equations of motion, as it is done in MD, the KMC method is based on the assumption that the long-time dynamics of a system consists of diffusive jumps from state to state. Each of the states is treated independently, which makes KMC a very efficient method. The dynamics of the system, that is, the probability of transition from one state to another does not depend on the history of the system. The probability of a state-to-state transition is assigned randomly and the most probable transition is statistically chosen. This allows avoiding the complications related to the choice of interatomic potentials, thus overcoming the time limitations of MD simulations (usually $t < 1$ μs) and accessing the macroscopic length scale. KMC is used as an extension of MD to further evolve the damage cascade in time and study the diffusion, accumulation, and annihilation of defects after a collision cascade took place [155].

To further extend the problem into the macro-domain, the DD [128] and FEM [129, 156] methods, based on dividing a geometrical space on a number of finite (non-overlapping) segments, are usually applied. FEM has been used to study the response of a macro-object to external stress in engineering and has also been applied to study the behavior of solids under irradiation by extrapolating the known displacements and evaluating the geometry of a 3D object. DD method allows for calculating the motion of dislocations as well as evaluating the plastic deformation in the material induced by the collective motion of dislocations.

5.2 *Ab initio* molecular dynamics: coupling MD with density functional theory

AIMD is one of the most important tools in quantum physics and chemistry [157]. In a typical AIMD simulation, it is assumed that the system consists of N nuclei and N_e electrons for which the Born-Oppenheimer (BO) approximation is applied [158]. The BO approximation implies that the dynamics of the electronic and nuclear subsystems can be treated separately given the fact that the nuclei are much heavier than the electrons and thus the time scales of their motion are very

different. In AIMD, the nuclei are evolved using classical mechanics, while the electronic ground state is adapted to the instantaneous nuclear positions at each step of the dynamics (i.e., the *adiabatic* approximation). The ground-state electronic problem is taken into account through advanced methods, most commonly from DFT [125, 159], a quantum-mechanical method that is used to calculate the electronic structure of many-body systems. Given its importance in describing physical and physicochemical properties of materials, and as it is functional to the understanding of the next section, a brief introduction to the main concepts of DFT is given here.

Practical DFT calculations are based on the Kohn-Sham (KS) formalism [126], which replaces the complex problem of interacting electrons in the standard Schrödinger equation by a problem of non-interacting electrons moving in an effective potential V_{eff}:

$$\left\{-\frac{1}{2}\nabla^2 + V_{\text{eff}}([n],\mathbf{r})\right\}\psi_i^{\text{KS}}(\mathbf{r}) = \varepsilon_i\psi_i^{\text{KS}}(\mathbf{r}), \tag{1}$$

where ε_i is the eigenvalues of the KS equations and ψ_i^{KS} is the one-electron KS wave functions. Here, the effective potential $V_{\text{eff}}([n],\mathbf{r}) = V_{\text{ext}}(\mathbf{r}) + V_{\text{H}}([n],\mathbf{r}) + V_{\text{xc}}([n],\mathbf{r})$ includes the external potential $V_{\text{ext}}(\mathbf{r})$ in which the electrons move (i.e., the electron-nuclei Coulomb attraction), the exchange-correlation (XC) potential $V_{\text{xc}}([n],\mathbf{r})$, in which all the many-body effects are included, and the Hartree potential $V_{\text{H}}([n],\mathbf{r})$ which is the electrostatic potential created by the electron density. The solution to self-consistent KS equations Eq. (1), is the exact electron density of the system of interacting electrons, provided that V_{eff} is known exactly: $n(\mathbf{r}) = \sum_{i=1}^{N}\left|\psi_i^{\text{KS}}(\mathbf{r})\right|^2$. All the properties of the system (e.g., electronic structure and ground-state energy) can be determined from the electron density, according to the Hohenberg-Kohn theorem [125].

AIMD is used to simulate any physicochemical process where the electronic structure of the system changes significantly or when a detailed description of the structure is needed. A typical example would be the simulation of chemical reactions, where chemical bonds are formed or broken, which cannot be described via classical force fields.

5.3 Time-dependent density functional theory for electron dynamics and its coupling to MD

Although the adiabatic BO approximation is the usual approximation in the methods described above, its applicability is only justified in near-equilibrium situations. However, under ion impact, the electronic subsystem is rapidly driven out of equilibrium.

A realistic description of the dynamics of the electrons in the target during the passage of fast ions can be obtained in the framework of TDDFT which gives access to the electron dynamics out of the electronic ground state. In particular, real-time TDDFT [160] provides a non-perturbative description of the electronic excitations upon an external perturbation and can be combined with the Ehrenfest MD scheme [161], which allows for coupling between electron and ion motion, contrary to the BO picture.

TDDFT consists in solving the time-dependent KS equations [123]:

$$i\hbar\frac{\partial}{\partial t}\psi_i^{\text{KS}}(\mathbf{r},t) = \left\{-\frac{\hbar^2\nabla^2}{2m} + \hat{V}_{ext}(\{R_I(t)\}) + \hat{V}_{HXC}[n(\mathbf{r},t)]\right\}\psi_i^{\text{KS}}(\mathbf{r},t), \tag{2}$$

where $\hat{V}_{HXC}$ describes both the electrostatic (Hartree) electron-electron interaction and the quantum-mechanical XC potential, $\hat{V}_{ext}$ is the potential arising from the ions (both the fast-moving impacting particle and the target atoms), and $\{R_I(t)\}$ are the atomic positions. The force on the nuclei in Ehrenfest dynamics is defined as

$$F_I(t) = -\sum_i \left\langle \psi_i^{\mathrm{KS}}(t) | \nabla_{R_I} \hat{H}_e | \psi_i^{\mathrm{KS}}(t) \right\rangle \tag{3}$$

where $\hat{H}_e$ is the Hamiltonian, that is, the operator on the r.h.s. of Eq. (2). Ehrenfest dynamics is a mean-field method, meaning that the nuclei move on an effective potential energy surface (a mathematical function that describes the energy of the system and whose value depends on the coordinates of all the atoms), which is an average of all adiabatic states involved, weighted by their populations. Other methods exist, in particular, one allowing for electronic transitions, that is, switches between adiabatic states when their population changes [162].

The solution of the time-dependent KS equations in real time can be obtained by applying the so-called time-evolution operator, evolving the KS states in time [123]. The time-step of this propagation must be of the order of attoseconds to describe the fast dynamics of the electrons, in contrast to what occurs in AIMD and MD where the time-step is of the order of femtoseconds. The time-dependent electron density is calculated at each step, from which the total energy of the system is obtained. Knowing the total energy as a function of time, the electronic stopping power can be calculated as $S_e = -dE/dx$, where dE is the energy loss and dx is the distance traveled by the projectile inside the target.

Many examples of accurate first-principles calculations of the electronic stopping power are available in the literature [117, 118, 163–168]. Recent studies have demonstrated that electronic excitations (induced by both the primary impacting ion and especially by PKAs and further displaced atoms) affect the cascade evolution [118, 169–171] and thus, they need to be accounted for. The electronic stopping effects can be included in MD cascade simulations through the so-called two-temperature (2T) model [118, 172]. In 2 T-MD, the electrons are included as a thermal bath. Each particle is subject to a friction force representing the electronic stopping and a stochastic force representing the coupling between the vibrational degrees of freedom of the lattice and the electrons. This model considers constant electronic density in the entire system and thus, the electronic stopping power is independent of the crystal direction. Recent studies have extended the 2T model by coupling the electronic and nuclear effects via many-body forces that act in a correlated way. This allowed for the construction of a unified model for ion-electron interactions [170, 171, 173, 174] with a complex energy-exchange process between the ionic and electronic subsystems [174].

6. Selected cases of radiation damage studies in materials relevant for exploration of the Moon

The previous section provided an overview of computational methods that can be applied to study radiation damage in materials and discussed the advantages of combining such methods into a multiscale approach. This section mainly focuses on the effects of radiation on materials of practical use on the Moon, including several novel and promising materials. We overview the existing radiation damage studies for these novel materials, emphasizing multiscale modeling when available.

6.1 Improving the model for solar cell degradation via a multiscale approach

Generally, degradation of solar cells is modeled via the non-ionizing energy loss (NIEL) approach, the NIEL being the portion of energy loss per unit path length of the projectile converted into displacement damage. According to Akkerman et al. [175] (the definition used in most simulation tools), the NIEL is defined as:

$$\mathrm{NIEL}(E) = \frac{N_A}{A}\int_{T_d}^{E_{\max}} Q(E_R)E_R\left(\frac{d\sigma}{dE_R}\right)_E dE_R = \frac{N_A}{A}D(E), \tag{4}$$

where E is the total kinetic energy of the external particle, E_R is the portion of kinetic energy which turns into displacement damage, $Q(E_R)$ is the partition factor giving the fraction of kinetic energy to be lost to NIEL mechanisms, N_A is Avogadro's number, A is the atomic mass of the lattice atom, $d\sigma/dE_R$ is the partial differential cross section for creating a recoil atom with energy E_R, and $D(E)$ is the displacement damage function. The integral runs from the minimum energy required to permanently displace an atom to a defect position, that is, the threshold displacement energy T_d, to $E_{\max}$, which is the maximum energy transferred to a recoil atom in a particular interaction. Although the NIEL concept differs from the nuclear stopping power, as it includes also the energy loss to non-ionizing events induced by hadronic interactions, as already mentioned above (see **Table 2**), relevant non-ionizing effects are induced by particles with energies from few to few tenths of MeV, which is the regime of Coulomb interactions.

On the basis of a large set of experimental observations, it is assumed that the degradation of a semiconductor device under irradiation can be linearly correlated with the NIEL [176]. In practice, this means that the number of defects should give a measure of the damage irrespective of their distribution, whether clustered in high density in small regions (as in the case of neutron damage) or homogeneously scattered over a relatively wide volume (as in the case of the low-energy proton or γ-ray-induced damage) [177]. Thus, in principle, the damage produced by different particles (with different energies) should be scalable via their NIEL (i.e., the number of displacements), as indeed has been shown in several studies [176, 178–182]. The NIEL scaling is a powerful method for dealing with displacement damage predictions in complex radiation environments, such as on the Moon and in space missions in general. However, deviations from the linearity exist and seem to be associated with the "quality" of the radiation damage at the microscale as induced by different kinds of particles and (or) as influenced by intrinsic defects in the target [183].

Generally, the NIEL is calculated via MC particle transport codes, assuming amorphous target materials, a static T_d that is constant for each element in all the materials where such element is found (thus, not considering the underlying electronic structure), and a simple linear collision cascade model for the number of final defects [184]. Several quantities in the NIEL formula and, more generally, the overall understanding of radiation damage can be strongly improved via AIMD and TDDFT+MD studies. T_d, for example, is an important quantity that can significantly affect the NIEL [185, 186] and its accurate estimation can be accessed by AIMD simulations [187, 188]. Recent results for T_d in semiconductors have shown that the electronic excitations can, in general, reduce their value [122], in line with previous experimental results [189]. The effect of electronic excitations consists in weakening the atomic bonds making it easier to displace an atom from its equilibrium position. On the other hand, the "heating" effect of electronic excitations has the consequence of facilitating the healing of the structure. Even a small change in T_d affects the calculated NIEL, as can be seen in **Figure 3** showing the NIEL for a

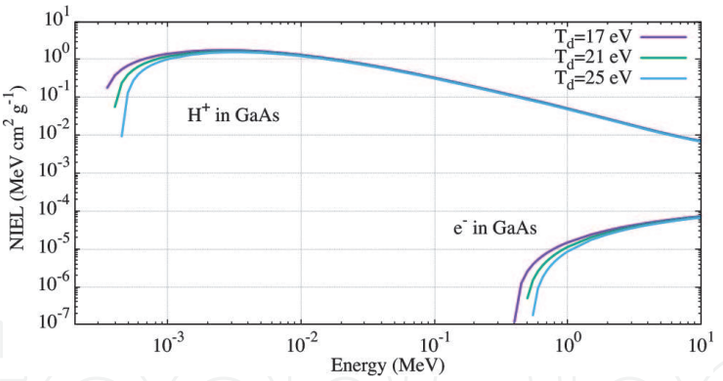

Figure 3.
NIEL for protons and electrons in GaAs for different values of the threshold displacement energy T_d calculated with the online SR-NIEL tool [190].

proton and an electron in GaAs. The NIEL is affected by the choice of T_d in an energy window of the lunar radiation environment (see **Table 1**). These findings raise an important question about the role of electronic excitations in defect formation that deserves more attention in future works.

Another example of possible improvement in the NIEL model is a more precise calculation of the number of radiation-induced defects and of the "quality" of radiation-induced damage (which type of defects are induced). It has been observed that point-like and clustered defects contribute differently to some degradation parameters [191]. Recent MD studies [192–194] and experimental works [181, 195, 196] have proposed an effective or *adjusted* NIEL to correct the deviations from a linear dependence of degradation parameters on the NIEL and restore a linear relationship. Other MD studies [197] proposed new metrics for counting defects including the effect of a "heat spike", which leads to a much lower rate of final defects as compared to predictions from a simple linear collision cascade model as commonly used in the NIEL calculations based on MC particle transport [184, 198].

On a parallel research stream, multiscale studies in a number of materials combining MD simulations of collision cascades with the electronic stopping from TDDFT offer a more accurate description of both the number and the nature of defects created under realistic conditions. The electronic degrees of freedom and their coupling to the phonons of the target affect the cascade evolution and morphology [170, 171, 173, 174]. This is of relevance for the NIEL which includes a part of energy dissipated to phonons. This fraction depends on the energy of the impinging particle but also on the properties of the material. Some studies have shown that the direction-dependence of the electronic stopping can influence the collision cascades [118]. Other studies have demonstrated that the formation of thermal spikes and therefore of amorphous pockets is sensitive to the electronic specific heat [199] and others that the choice of the model employed for the inclusion of the electronic effects and in particular the overestimation (or underestimation) of electron-phonon coupling can have a significant influence on the number of defects created [171].

6.2 Radiation effects in the next-generation lightweight photovoltaic panels

As discussed in Section 2, HOIPs have a unique combination of properties particularly interesting for lunar exploration. The general chemical formula for perovskites is ABX_3, where A and B are two metal ions with different ionic radii and X is an anion that is six coordinated to the B-site [200]. HOIPs, in particular,

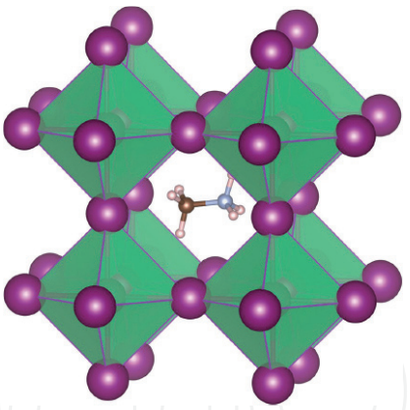

Figure 4.
Structure of a HOIP: methylammonium cation ($CH_3NH_3^+$) occupies the central A site surrounded by 12 nearest-neighbor iodide ions in corner-sharing PbI_6 octahedra [201] (available under the terms of the creative commons CC BY license).

comprise a negatively charged lead-halide inorganic skeleton where B is a metal cation (Sn^{2+} or Pb^{2+}), X is a halide anion (I^-, Br^-, and/or Cl^-) and A is a monovalent positively charged organic cation, such as methylammonium ($MA^+ = CH_3NH_3X^+$, where X = I, Br, Cl) or formamidinium ($FA^+ = CH(NH_2)_2^+$ (**Figure 4**).

Despite many advantages, several external factors, such as air, moisture [202], UV light [47, 203], heat, light soaking [204], and partially also radiation [205, 206], induce considerable structural instabilities in HOIPs. An intrinsic instability is also present, caused by a relatively weak cohesion between the organic cation and the inorganic octahedra and predominantly by the low-energy barriers for the migration of halide anions and organic cations, with halide migration being the most prevalent [201, 207–210]. Phase segregation can be induced by large-scale ion migration [211]. However, some of the challenges that HOIPs-based solar cells face on Earth, such as degradation caused by moisture, are not relevant for space applications [212]. Thermal and vacuum stability, high power-conversion efficiency, and radiation resistance are the main challenges in the space context. A sensible choice of the chemical composition, of eventual use in tandem devices [212] (which also helps to reach an efficiency of up to 30%) or incorporation of a functionalized 2D metal-organic frameworks (MOFs) [213], can improve the long-term operational stability of HOIPs.

A relevant collection of DFT studies for HOIPs can be found in Ref. [214]. A recent study based on DFT + compressed sensing-symbolic regression has shown that mitigation of the propensity of halogens to migrate could be achieved by selectively strengthening specific bonds [215]. The study also unveiled the reasons for improved stability given by specific halogens, the origin of the higher stability offered by certain organic cations compared to others, and highlighted in a quantitative and first-principles manner how weak interactions have a significant role in binding the halogens more strongly.

The study of the radiation tolerance of perovskite solar cells is an extremely active field of research. Solar cells based on HOIPs as active layers have been recently sent to space via first campaigns [60, 216]. Several ground-testing experiments have been performed mostly using protons, either with an energy of several tenths of MeV [69, 211, 217] or with an energy of 150 keV, 100 keV, and 50 keV [70, 218, 219], of less relevance for realistic space conditions.

Superior radiation resistance of perovskite solar cells in comparison to commercially available crystalline Si-based cells has been demonstrated [69]. Moreover, experiments have shown that perovskite solar cells have remarkable self-healing

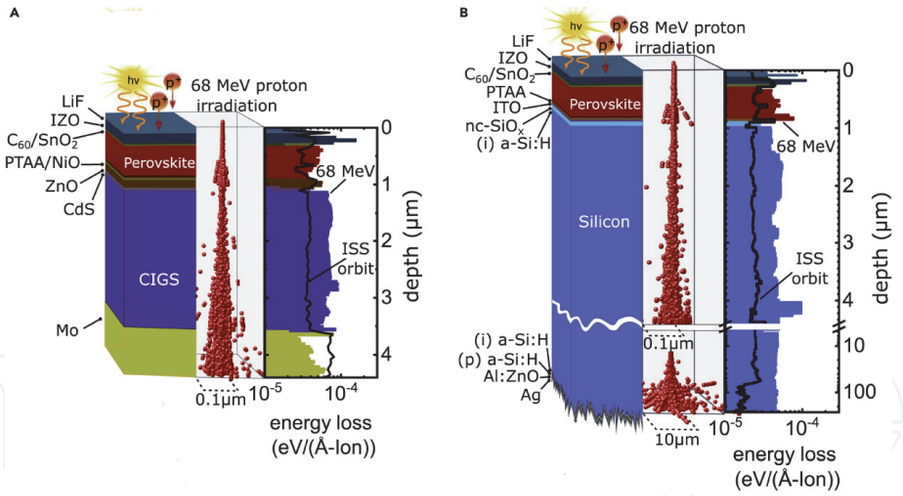

Figure 5.
3D scatter plots of the straggling of 68 MeV protons within the (A) HOIP/CIGS($Cu(In,Ga)Se_2$) and (B) HOIP/SHJ(Si heterojunction) tandem solar cells. The energy loss of the incident 68 MeV protons to recoils is plotted as a function of depth based on SRIM simulations with a total of 5×10^7 protons. The damage of a real space environment at the orbit of the ISS is shown as a black line. Adapted from [90] (available under the terms of the Creative Commons CC-BY license).

capabilities (at room temperature) that lower the number of defects caused by proton irradiation [69]. Another experimental study has shown that the proton irradiation effects on the physical properties of HOIPs are strongly dependent on the synthesis method [220] which appeared to affect the strength of specific chemical bonds. In particular, HOIPs, produced by mechano-chemical synthesis, have shown practically no change in their physical properties after irradiation with a high-energy 10 MeV proton beam with doses of up to 10^{13} protons/cm^2.

Recently, multi-junction tandem solar cells (combining HOIPs with previous technologies or technologies investigated in parallel) have also been studied under ion irradiation [217]. Lang et al. [217] carried out SRIM simulations of energy loss of high-energy protons as well as the energy transferred to the recoiling nuclei—a measure of the degradation of PV parameters—in tandem solar cells (**Figure 5**). The study [217] has shown that HOIP/CIGS tandem solar cells possess a high radiation hardness and retain over 85% of their initial performance even after 68 MeV proton irradiation and a dose of 2×10^{12} proton/cm^2, equivalent to 50 years in space at the International Space Station (ISS) orbit.

First-principles calculations of the atomic knock-on displacement events in HOIPs have shown that such displacements are significant and highly energy-dependent [221]. The work has shown that only certain types of atoms are prone to displacements suggesting that mitigation strategies should be directed toward some chemical species more than others. Overall, further studies are necessary, but existing research proves that HOIPs-based solar cells have a remarkable potential for power generation on missions to low Earth orbit, the Moon, and beyond [62].

6.3 Novel multi-principal-element alloys with enhanced radiation resistance

6.3.1 Outstanding properties of MPEA for space applications

Another promising class of novel materials for space applications is multi-principal element alloys (MPEAs) [222, 223], which combine superior mechanical properties and enhanced radiation resistance [224]. Also known as high-entropy alloys (HEAs) or concentrated solid-solution alloys (CSSAs), MPEAs consist of at least five principal elements with the concentration of each element from 5 to 35%

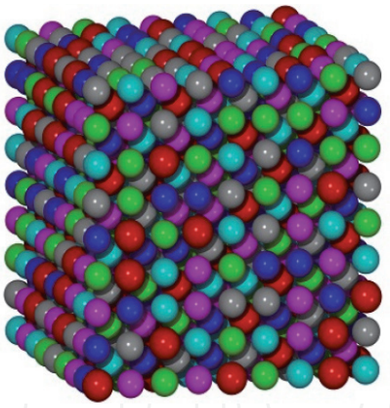

Figure 6.
Atomic structure of a body-centered cubic (BCC) AlCoCrCuFeNi HEA. The Al, Fe, Co, Cr, Ni, and Cu atoms are shown in red, magenta, green, blue, cyan, and gray colors, respectively [225] (available under the https://creativecommons.org/licenses/by-nc-sa/3.0/Creative Commons Attribution License).

[222]. Despite the complex composition, MPEAs often form single-phase solid solutions (**Figure 6**). The interest of researchers in MPEAs has been growing exponentially in recent years, as they exhibit a paradigm shift in alloy development. MPEAs indeed combine a set of outstanding properties, such as high strength, hardness, fracture toughness, corrosion resistance, strength retention at high temperature [226], good low-temperature performance [227], and recently discovered enhanced radiation resistance, superior to conventional alloys and pure metals [149, 222, 223, 228–233]. Moreover, MPEAs have great potential as 3D printing materials [234]. MPEAs can be printed from a powder, providing manufacturing freedom for lightweight and customizable products of complex geometries for applications in the aerospace, energy, molding, tooling, and other industries, all of the great relevance for the exploration of the Moon.

Recent experiments have shown that MPEAs have a higher resistance to defect formation due to high atomic-level stress and chemical heterogeneity [235]. MPEAs also possess lower void swelling and higher phase stability [236, 237] as compared to conventional alloys. Self-healing capability is another remarkable property of MPEAs [227, 236, 238].

The subclass of lightweight (LW) MPEAs have a great potential for space applications due to their high strength-to-weight ratio [239–241]. The main components of LWMPEAs are low-density elements, such as Al, Mg, Si, and Ti [240]. The latter is of extreme importance for ISRU since 99% of the lunar soil consists of Si, Al, Ca, Fe, Mg, and Ti oxides [5, 242].

Currently, the main focus of computational studies has been on the single-phase random solid-solution (SS) alloys based on transition metals with high densities (Co, Cr, Fe, Ni) for application in radiation environments, in particular in nuclear reactors [148, 149, 232, 236, 243–245]. MD simulations of displacement cascades applied to pure metals and multicomponent alloys [150, 244–248] confirm the experimentally observed reduction of the number of defects and defect clusters in MPEAs compared to pure metals (**Figure 7**).

The electronic stopping power for a proton in binary alloys has recently been calculated using real-time TDDFT [249]. The study has shown that the electronic stopping power of binary alloys is higher than that of pure Ni, suggesting that alloys more effectively stop the incoming particles. Moreover, the inclusion of the electronic stopping into MD simulations of defect formation significantly reduces the final number of surviving defects, as shown in **Figure 8**. The inclusion of both the electron-phonon coupling and the electronic stopping in the 2T-MD model not only reduces the actual number of defects but also notably impacts their final

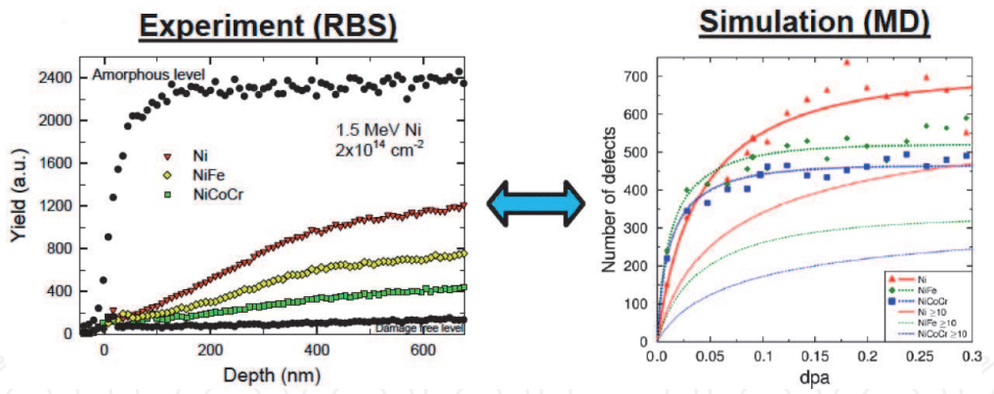

Figure 7.
The number of defects in Ni, NiFe, and NiCoCr from experiments and MD simulations [150].

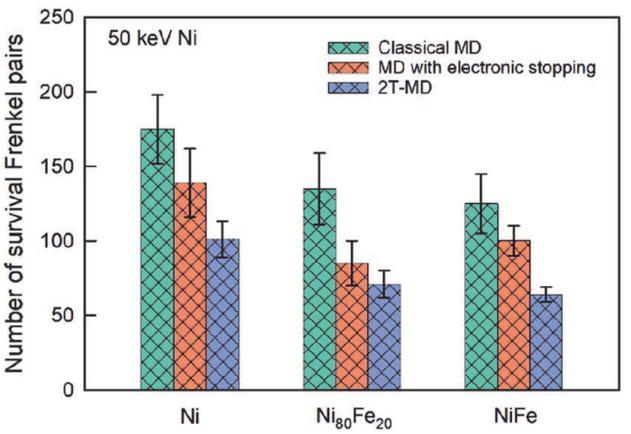

Figure 8.
Average number of surviving defects in the classical MD cascade, MD cascade including electronic stopping force, and the 2 T-MD cascade at the end of the simulation for 50 keV Ni cascade in Ni, $Ni_{80}Fe_{20}$, and NiFe [224, 250–252].

arrangement, namely leading to more isolated point defects and reducing the size of defect clusters in binary and ternary alloys [250–254].

The majority of MD studies focus on binary and ternary MPEAs due to the lack of force fields for alloys with more than three elements. However, some studies exist [233] on defect formation in NiCoFeCr alloy in which fewer defects have been found at the end of the displacement cascade with PKA energies from 10 to 50 keV, as compared with pure Ni. The limitations of the classical MD with force fields and the ways of solving this problem are discussed in the following.

6.3.2 Machine-learning assisted materials discovery

Classical MD with empirical potentials is the method that proved to work well for large systems and long time scales [139] for the modeling of collision cascades. However, classical interatomic potentials cannot accurately reproduce interactions between the atoms in MPEAs due to their complex structure and lattice distortions leading to internal strain [149, 255, 256]. On the other hand, *ab initio* methods relying on quantum mechanics, such as DFT, can accurately reproduce the interatomic potentials in complex structures but are limited to a small length scale.

Recent developments in machine learning (ML) approaches can provide a solution to this problem. ML-enhanced materials discovery is an emerging and extremely rapidly growing field. The combination of a precise model based on quantum mechanics and ML algorithms have the potential for an efficient and

accurate description of materials properties [257–259]. Much progress has been made in recent years in the development of ML-based interatomic potentials with the input from electronic structure calculations. First applications have shown that accurate potentials can be obtained for many relevant systems [260–265]. ML-assisted calculations have been applied to pure metals, binary, ternary alloys [266, 267], and MPEAs [268–270].

ML and artificial intelligence (AI) may become powerful tools for more accurate multiscale modeling of materials properties. Artificial Neural Networks (ANN) [271] combined with atomistic KMC have already been used to describe the microstructural changes in metals and alloys induced by irradiation [272]. Machine-learned interatomic potentials have been used to study defect formation in refractory MPEAs [273]. The results confirm experimental findings, showing that the 3D migration and increased mobility of defects in MPEAs promote defect recombination leading to more efficient healing. AI, thus, can provide a bridge between different methods, such as DFT, MD, and KMC, and allow for large-scale atomistic simulations of high accuracy, which will accelerate the discovery of new advanced materials.

6.4 Radiation resistance of fiber-reinforced polymers and composites for habitats

Fiber-reinforced polymers (FRPs) are composite materials made of a polymer matrix reinforced with fibers. Typical polymers that are often used include epoxy, vinyl ester, polyester thermosetting plastic, and phenol-formaldehyde resins. Typical fibers include, but are not limited to, glass, carbon, and aramid. In a composite FRP material, the polymer and fiber often have significantly different physical and/or chemical properties, which remain separate and distinct within the finished structure but are complementary for tailored properties [274]. Because of their low density (lightweight), great moldability, specific strength, stiffness [275], excellent mechanical stability, and good thermal properties, FRPs are being increasingly used as structural materials in aerospace, automotive, marine industries, and civil infrastructures. Hence, FRPs are of great interest for many applications for lunar missions as potential structural materials [276]. Glass fibers (also "fiberglass") can be directly produced from the lunar soil as well as from by-products of metal extraction and can be used to reinforce lunar concrete [277].

The radiation environment on the Moon presents challenges for FRPs with concerns on both the immediate reactions taking place in the materials (short-term effects) and continued post-exposure degradation processes (long-term effects) [276, 278]. In the past decades, many selected FRPs have been ground-tested at different kinds of radiation and particle accelerator facilities for their potential use in space-related radiation environments, including UV-light [279, 280], γ-rays [281, 282], electron beams [283, 284] and proton beams [285].

Carbon-fiber composites have been widely used in aerospace industries due to their high-temperature stability and low density along with high strength, as well as superior beam-induced shock absorption [285, 286]. A combined modeling and experimental study of the radiation effect on carbon-fiber-reinforced molybdenum-graphite compound (MoGRCF) [285], including MC simulations of the energy deposited into a realistic structure by a 200-MeV proton beam (**Figure 9**) has show that carbon-fiber-reinforced composites have superior beam-induced shock absorption ability compared to that of graphite.

In the 1980s, the degradation behavior of carbon-fiber-reinforced plastic (CFRP) under electron beam irradiation in various conditions simulating experiments in space has been studied by Sonoda et al. [283]. It has been observed that

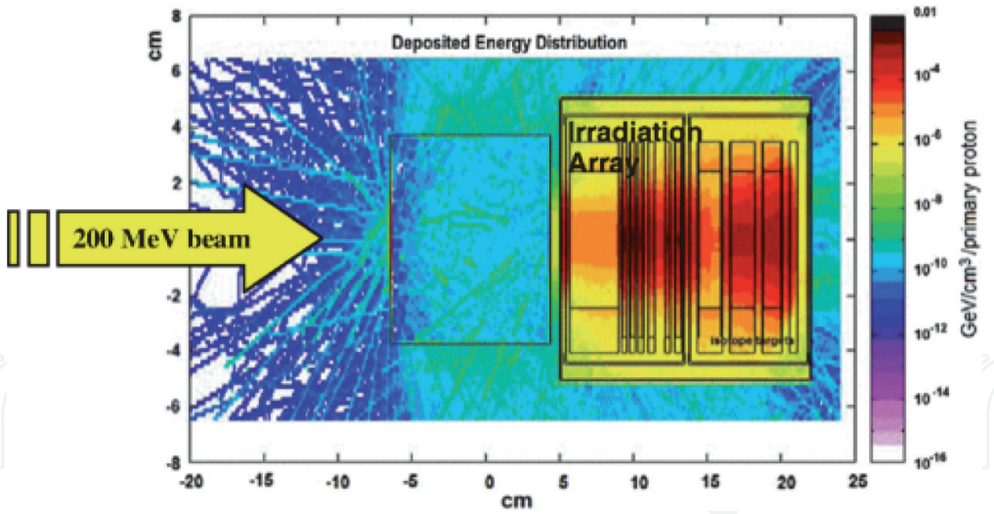

Figure 9.
MC modeling of the energy deposition for a 200-MeV proton beam interacting with an irradiation target array (MoGRCF) in tandem with the isotope production array downstream [285] (available under the terms of the Creative Commons Attribution 3.0 License).

there is no change in mechanical properties of CFRP when irradiated by up to a dose of 50 MGy. MC simulations of radiation effects in FRPs have shown that by adding lead nanoparticles it is possible to increase their radiation resistance [287]. According to the study, the addition of 15 wt% of lead nanoparticles to FRPs led to a mass reduction of ~64% for the same level of radiation shielding.

An alternative to glass fiber for polymer reinforcement is basalt fiber which offers advantages, such as high specific mechanical and physicochemical properties, biodegradability, non-abrasive qualities, and cost-effectiveness [288]. Arnhof et al. [289] have recently studied mechanical properties of fiber-reinforced geopolymer (FRG) with basalt fiber (i.e., inorganic alumino-silicate polymer) made from lunar regolith simulant as potential shielding and structural material. As basalt fibers can be produced *in situ* at the lunar surface efficiently, they can be used widely to increase the mechanical strength of geopolymers. Overall, geopolymers are advantageous for lunar construction due to their excellent resistance to extreme temperature fluctuations and adequate shielding from radiation [290], as well as enhanced mechanical properties over conventional cement [291].

The additive-manufacturing (AM) techniques for lunar construction from regolith, including FRP materials, and their suitability for ISRU has recently been reviewed in Refs. [292, 293]. The AM techniques for lunar construction include Cement Contour Crafting (CCC), Binder Jetting (BJ), Selective Solar Light Sintering (SSLS) and Selective Laser Sintering/Melting (SLS/SLM) for 3D printing and metal melting, Stereolithography/Digital Light Processing (SLA/DLP), among others. CCC and BJ technologies could be used for outdoor lunar civil engineering. SSLS could be applied to both direct compacting of lunar regolith to ceramic parts and 3D printing. SLA/DLP-based methods could be used for the indoor manufacturing of ceramic instruments, providing higher precision and printing quality and lower defect rate of the printed parts than other AM methods. In the last decade, studies have clearly shown that the 3D-printing technologies will become one of the cornerstones of lunar exploration, providing future astronauts with all the necessary infrastructure [293].

Lunar concrete consisting of mined regolith with the addition of glass fibers (also made *in situ* from regolith containing plenty of silicates) has a high strength-to-weight ratio and can be easily 3D-printed, as tests on lunar regolith simulant have shown [294]. Other studies have shown the promising properties of urea from

astronauts' urine as a superplasticizer for lunar geopolymers for 3D-printing applications. The use of urea is expected to reduce the necessary amount of water by about 30% [295].

It is worth mentioning that the 4D printing of a "smart material" with FRPs that responds to radiation-induced damages and aging in a programmable way could be realized in near future [296, 297]. In addition to experiments on the radiation environment in a lab, multiscale computational simulations as mentioned above could be helpful for gaining further insights into the radiation-induced molecular changes occurring in polymers.

7. Conclusions

In this chapter, we introduced some relevant materials for lunar habitat construction and power generation. We discussed the radiation environment on the Moon and the effects that radiation can cause in such materials. We provided an overview of computational methods used to study different stages of radiation damage in materials, focusing on the methods that allow simulating the behavior of materials with extreme accuracy down to the atomic scale. We emphasized that by coupling different methods, it is possible to account for different time and length scales in the evolution of the radiation-induced effects and to combine the electronic effects with atomic displacements.

Several particular examples of radiation damage studies have been discussed with the focus on novel materials with enhanced radiation resistance and other remarkable properties for use on the Moon that can revolutionize space exploration. Such materials include HOIPs for energy production and MPEAs and FRP composite materials for construction. The primary materials considered for lunar construction are FRGs with basalt or glass fibers, which have excellent mechanical properties, can benefit from ISRU, and provide necessary radiation shielding. We emphasized that researchers' effort is mainly directed toward the development of additive manufacturing techniques, such as 3D printing for habitat construction from lunar regolith. 3D printing will allow producing complex and customizable products in a shorter time and with a lower cost and material consumption.

Nowadays, the radiation-induced effects in materials for space missions are mainly studied by MC particle transport modeling, inheriting the remarkable modeling and computational efforts by the high-energy physics community. However, with the development of first-principles methods and multiscale simulations, a more accurate understanding of radiation effects in materials can be achieved for the regime below hadronic interactions, with details down to atomic scale. It can be expected that the combination of first-principles methods, MC particle transport, and ML will contribute further to the investigation of materials to unravel their full potential for the application in harsh space radiation environments, in particular for what concerns the resistance and resilience to cumulative displacements effects.

Acknowledgements

The authors are grateful for the funding provided by the project ESC2RAD within the Horizon 2020 Research and Innovation program (grant agreement ID: 776410) and by the project PROIRICE within the program H2020-MSCA-IF 2016 of the Horizon 2020 program of the European Union (grant agreement ID: 748673).

Author details

Natalia E. Koval[1*], Bin Gu[2,3], Daniel Muñoz-Santiburcio[1,4] and Fabiana Da Pieve[5]

1 CIC Nanogune BRTA, San Sebastián, Spain

2 Jiangsu International Joint Laboratory on Meteorological Photonics and Optoelectronic Detection, Nanjing University of Information Science and Technology, Nanjing, China

3 Atomistic Simulation Centre, Queen's University Belfast, Belfast, United Kingdom

4 Instituto de Fusión Nuclear "Guillermo Velarde", Universidad Politécnica de Madrid, Spain

5 Royal Belgian Institute for Space Aeronomy BIRA-IASB, Brussels, Belgium

*Address all correspondence to: natalia.koval.lipina@gmail.com

References

[1] Crawford IA, Anand M, Cockell CS, Falcke H, Green DA, Jaumann R, et al. Back to the Moon: The scientific rationale for resuming lunar surface exploration. Planetary and Space Science. 2012;**74**(1):3-14. Scientific Preparations For Lunar Exploration

[2] Off-Earth Manufacturing Symposium: How to Build a New Home in Space. 2021. Available from: https://www.esa.int/Enabling_Support/Preparing_for_the_Future/Discovery_and_Preparation/Off-Earth_manufacturing_symposium_how_to_build_a_new_home_in_space [Accessed: December 12, 2021]

[3] NASA's Plan for Sustained Lunar Exploration and Development. 2020. Available from: www.nasa.gov/sites/default/files/atoms/files/a_sustained_lunar_presence_nspc_report4220final.pdf [Accessed: December 12, 2021]

[4] NASA's Lunar Exploration Program Overview. 2020. Available from: https://www.nasa.gov/sites/default/files/atoms/files/artemis_plan-20200921.pdf [Accessed: December 12, 2021]

[5] Stefanescu DM, Grugel RN, Curreri PA. In situ resource utilization for processing of metal alloys on Lunar and Mars BASES. In: Space 98. Albuquerque, MN: American Society of Civil Engineers; 1998. pp. 266-274

[6] Zacny K. Lunar drilling, excavation and Mining in Support of science, exploration, construction, and In situ resource utilization (ISRU). In: Badescu V, editor. Moon: Prospective Energy and Material Resources. Berlin Heidelberg, Berlin, Heidelberg: Springer; 2012. pp. 235-265

[7] Just GH, Smith K, Joy KH, Roy MJ. Parametric review of existing regolith excavation techniques for lunar in situ resource utilisation (ISRU) and recommendations for future excavation experiments. Planetary and Space Science. 2020;**180**:104746

[8] Sacksteder K, Sanders G. In-situ resource utilization for Lunar and Mars exploration. AIAA 2007-345. 45th AIAA Aerospace Sciences Meeting and Exhibit; Reno, Nevada. US: NTRS; 2007

[9] Schreiner SS, Sibille L, Dominguez JA, Hoffman JA. A parametric sizing model for molten Regolith electrolysis reactors to produce oxygen on the Moon. Advances in Space Research. 2016;**57**(7):1585-1603

[10] Crawford IA. Lunar resources: A review. Progress in Physical Geography: Earth and Environment. 2015;**39**(2):137-167

[11] Schwandt C, Hamilton JA, Fray DJ, Crawford IA. The production of oxygen and metal from lunar regolith. Planetary and Space Science. 2012;**74**(1):49-56. Scientific Preparations For Lunar Exploration

[12] Kozyrovska N, Lutvynenko TL, Korniichuk OS, Kovalchuk M, Voznyuk TM, Kononuchenko O, et al. Growing pioneer plants for a lunar base. Advances in Space Research. 2006;**37**:93-99

[13] Maggi F, Pallud C. Space agriculture in micro- and hypo-gravity: A comparative study of soil hydraulics and biogeochemistry in a cropping unit on earth, Mars, the Moon and the space station. Planetary and Space Science. 2010;**58**(14):1996-2007

[14] Ghidini T. Materials for space exploration and settlement. Nature Materials. 2018;**17**(10):846-850

[15] Pernigoni L, Lafont U, Grande AM. Self-healing materials for space applications: Overview of present

development and major limitations. CEAS Space Journal. 2021;**13**(3): 341-352

[16] Belvin W, Watson J, Singhal S. Structural concepts and materials for lunar exploration habitats. AIAA-2006-7338. AIAA Space 2006 Conference and Exposition; San Jose, CAL. US: NTRS; 2006

[17] Experimental Investigation of Selective Laser Melting of Lunar Regolith for In-Situ Applications. Volume 2A: Advanced Manufacturing of ASME International Mechanical Engineering Congress and Exposition, 11 2013. V02AT02A008

[18] Benaroya H. Lunar habitats: A brief overview of issues and concepts. REACH. 2017;**7-8**:14-33

[19] Bodiford M, Burks K, Perry M, Cooper R, Fiske M. Lunar in situ materials-based habitat technology development efforts at NASA/MSFC. In: Earth & Space 2006: Proceedings of 10th ASCE Aerospace Division International Conference on Engineering, Construction, and Operation in Challenging Environments. US: ASCE; 2006

[20] Ruess F, Schaenzlin J, Benaroya H. Structural design of a lunar habitat. Journal of Aerospace Engineering. 2006; **19**(3):133-157

[21] Rojdev K. Long term lunar radiation degradation of potential lunar habitat composite materials [PhD thesis]. 2012

[22] Meurisse A, Cazzaniga C, Frost C, Barnes A, Makaya A, Sperl M. Neutron radiation shielding with sintered lunar regolith. Radiation Measurements. 2020;**132**:106247

[23] Akisheva Y, Gourinat Y. Utilisation of Moon Regolith for radiation protection and thermal insulation in permanent lunar habitats. Applied Sciences. 2021;**11**(9):3853

[24] Miller J, Taylor LA, DiGiuseppe M, Heilbronn LH, Sanders G, Zeitlin CJ. Radiation shielding properties of lunar regolith and regolith simulant. LPI Contributions. 2008;**1415**:2028

[25] Montes C, Broussard K, Gongre M, Simicevic N, Mejia J, Tham J, et al. Evaluation of lunar regolith geopolymer binder as a radioactive shielding material for space exploration applications. Advances in Space Research. 2015;**56**(6):1212-1221

[26] Wang KT, Lemougna PN, Tang Q, Li W, Cui XM. Lunar regolith can allow the synthesis of cement materials with near-zero water consumption. Gondwana Research. 2017;**44**:1-6

[27] Toutanji H, Fiske MR, Bodiford MP. Development and Application of Lunar "Concrete" for Habitats. In: Earth & Space 2006: Engineering, Construction, and Operations in Challenging Environment. US: ASCE; 2006

[28] Lim S, Anand M. Space Architecture for Exploration and Settlement on Other Planetary Bodies: In Situ Resource Utilisation (ISRU) Based Structures on the Moon: Proceedings of the 2nd European Lunar Symposium; London, UK. 2014

[29] Meurisse A, Makaya A, Willsch C, Sperl M. Solar 3D printing of lunar regolith. Acta Astronautica. 2018;**152**: 800-810

[30] Cesaretti G, Dini E, De Kestelier X, Colla V, Pambaguian L. Building components for an outpost on the lunar soil by means of a novel 3D printing technology. Acta Astronautica. 2014;**93**: 430-450

[31] Shaw M, Humbert M, Brooks G, Rhamdhani A, Duffy A, Pownceby M. Mineral processing and metal extraction on the lunar surface—challenges and opportunities. Mineral Processing and

Extractive Metallurgy Review. 2021; **0**(0):1-27

[32] Dietzler D. Making it on the Moon: Bootstrapping Lunar industry. In: NSS Space Settlement Journal. Vol. 1. Washington, DC, USA: National Space Society; 2016

[33] Palos MF, Serra P, Fereres S, Stephenson K, González-Cinca R. Lunar isru energy storage and electricity generation. Acta Astronautica. 2020; **170**:412-420

[34] Ellery A. Generating and storing power on the moon using in situ resources. Proceedings of the Institution of Mechanical Engineers, Part G: Journal of Aerospace Engineering. 2021;**0**(0): 1-19

[35] Landis G, Bailey S, Brinker D, Flood D. Photovoltaic power for a lunar base. Acta Astronautica. 1990;**22**: 197-203

[36] Halbach E, Inocente D, Katz N, Petrov G. Solar Arrays with Variable Panel Elevations for the Moon Village. 2021

[37] Abhirama RK. Power generation system for lunar habitat. Technical Report. Technische Universität Berlin; 2020

[38] Kohout LL. Cryogenic Reactant Storage for Lunar Base Regenerative Fuel Cells: Proceedings of the International Conference on Space Power; Cleveland, OH. 1989

[39] Ellery A. Supplementing closed ecological life support systems with in-situ resources on the Moon. Life. 2021;**11** (8):770

[40] Bolonkin A. Inflatable Dome for Moon, Mars, Asteroids, and Satellites. AIAA-2007-6262. AIAA SPACE 2007 Conference & Exposition. Long Beach, California. US: NTRS; 2007

[41] Li J, Aierken A, Liu Y, Zhuang Y, Yang X, Mo JH, et al. A brief review of high efficiency III-V solar cells for space application. Frontiers in Physics. 2021;**8**:657

[42] Spitzer MB, Fan JCC. Multijunction cells for space applications. Solar Cells. 1990;**29**(2):183-203

[43] Torchynska T, Polupan G, Conde Zelocuatecatl F, Scherbina E. Application of iii-v materials in space solar cell engineering. Modern Physics Letters B. 2001;**15**(17-19):593-596

[44] Best Research-cell Efficiency Chart. 2021. Available from: www.nrel.gov/pv/cell-efficiency.html [Accessed: January 2021]

[45] Huang J, Yuan Y, Shao Y, Yan Y. Understanding the physical properties of hybrid perovskites for photovoltaic applications. Nature Reviews Materials. 2017;**2**(7):17042

[46] Schmidt-Mende L, Dyakonov V, Olthof S, Ünlü F, Lê KMT, Mathur S, et al. Roadmap on organic–inorganic hybrid perovskite semiconductors and devices. APL Materials. 2021;**9**(10): 109202

[47] Berry J, Buonassisi T, Egger DA, Hodes G, Kronik L, Loo Y-L, et al. Hybrid organic-inorganic perovskites (HOIPs): Opportunities and challenges. Advanced Materials. 2015;**27**(35): 5102-5112

[48] Wehrenfennig C, Eperon GE, Johnston MB, Snaith HJ, Herz LM. High charge carrier Mobilities and lifetimes in Organolead Trihalide perovskites. Advanced Materials. 2014;**26**(10): 1584-1589

[49] Brenner TM, Egger DA, Kronik L, Hodes G, Cahen D. Hybrid organic—inorganic perovskites: Low-cost semiconductors with intriguing

charge-transport properties. Nature Reviews Materials. 2016;**1**(1):15007

[50] Saba M, Quochi F, Mura A, Bongiovanni G. Excited state properties of hybrid perovskites. Accounts of Chemical Research. 2016;**49**(1):166-173

[51] Motta C, El-Mellouhi F, Sanvito S. Charge carrier mobility in hybrid halide perovskites. Scientific Reports. 2015; **5**(1):12746

[52] Ponseca CS, Savenije TJ, Abdellah M, Zheng K, Yartsev A, Pascher T, et al. Organometal halide perovskite solar cell materials rationalized: Ultrafast charge generation, high and microsecond-long balanced Mobilities, and slow recombination. Journal of the American Chemical Society. 2014;**136**(14): 5189-5192

[53] Stranks SD, Eperon GE, Grancini G, Menelaou C, Alcocer MJP, Leijtens T, et al. Electron-hole diffusion lengths exceeding 1 micrometer in an organometal trihalide perovskite absorber. Science. 2013;**342**(6156): 341-344

[54] Kojima A, Teshima K, Shirai Y, Miyasaka T. Organometal halide perovskites as visible-light sensitizers for photovoltaic cells. Journal of the American Chemical Society. 2009; **131**(17):6050-6051

[55] Yue L, Yan B, Attridge M, Wang Z. Light absorption in perovskite solar cell: Fundamentals and plasmonic enhancement of infrared band absorption. Solar Energy. 2016;**124**:143-152

[56] Snaith HJ. Perovskites: The emergence of a new era for low-cost, high-efficiency solar cells. The Journal of Physical Chemistry Letters. 2013; **4**(21):3623-3630

[57] Wei Z, Zhao Y, Jiang J, Yan W, Feng Y, Ma J. Research progress on hybrid organic–inorganic perovskites for photo-applications. Chinese Chemical Letters. 2020;**31**(12): 3055-3064

[58] Jeon NJ, Noh JH, Yang WS, Kim YC, Ryu S, Seo J, et al. Compositional engineering of perovskite materials for high-performance solar cells. Nature;**517** (7535):476-480

[59] Brown CR, Eperon GE, Whiteside VR, Sellers IR. Potential of high-stability perovskite solar cells for low-intensity-low-temperature (LILT) outer planetary space missions. ACS Applied Energy Materials. 2019;**2**(1): 814-821

[60] Cardinaletti I, Vangerven T, Nagels S, Cornelissen R, Schreurs D, Hruby J, et al. Organic and perovskite solar cells for space applications. Solar Energy Materials and Solar Cells. Aug 2018;**182**:121-127

[61] Yang J, Bao Q, Shen L, Ding L. Potential applications for perovskite solar cells in space. Nano Energy. 2020; **76**:105019

[62] Durant BK, Afshari H, Sourabh S, Yeddu V, Bamidele MT, Singh S, et al. Radiation stability of mixed tin–lead halide perovskites: Implications for space applications. Solar Energy Materials and Solar Cells. 2021;**230**: 111232

[63] Bailey S, Raffaelle R. Handbook of Photovoltaic Science and Engineering. Chichester, UK: John Wiley & Sons, Ltd; 2011. pp. 365-401

[64] Huang J, Kelzenberg MD, Espinet-González P, Mann C, Walker D, Naqavi A, et al. Effects of electron and proton radiation on perovskite solar cells for space solar power application. In: Proceedings of 2017 IEEE 44th Photovoltaic Specialist Conference (PVSC). Piscataway, NJ: IEEE; 2017. pp. 1248-1252

[65] Short K, Van Buren D. Printable Spacecraft: Flexible Electronic Platforms for NASA Missions. Technical Report. NASA Jet Propulsion Laboratory; 2012

[66] Kaltenbrunner M, Adam G, Głowacki ED, Drack M, Schwödiauer R, Leonat L, et al. Flexible high power-per-weight perovskite solar cells with chromium oxide–metal contacts for improved stability in air. Nature Materials. 2015;**14**(10):1032-1039

[67] Di Giacomo F, Fakharuddin A, Jose R, Brown TM. Progress, challenges and perspectives in flexible perovskite solar cells. Energy & Environmental Science. 2016;**9**:3007-3035

[68] Burschka J, Pellet N, Moon S-J, Humphry-Baker R, Gao P, Nazeeruddin MK, et al. Sequential deposition as a route to high-performance perovskite-sensitized solar cells. Nature. 2013;**499**(7458):316-319

[69] Lang F, Nickel NH, Bundesmann J, Seidel S, Denker A, Albrecht S, et al. Radiation hardness and self-healing of perovskite solar cells. Advanced Materials. 2016;**28**(39):8726-8731

[70] Miyazawa Y, Ikegami M, Miyasaka T, Ohshima T, Imaizumi M, Hirose K. Evaluation of radiation tolerance of perovskite solar cell for use in space. In: Proceedings of 2015 IEEE 42nd Photovoltaic Specialist Conference (PVSC). Piscataway, NJ: IEEE; 2015. pp. 1-4

[71] Miyazawa Y, Ikegami M, Chen H-W, Ohshima T, Imaizumi M, Hirose K, et al. Tolerance of perovskite solar cell to high-energy particle irradiations in space environment. iScience. 2018;**2**:148-155

[72] Matthewman R, Crawford IA, Jones AP, Joy KH, Sephton MA. Organic matter responses to radiation under lunar conditions. Astrobiology. 2016; **16**(11):900-912

[73] Lucey P, Korotev RL, Gillis JJ, Taylor LA, Lawrence D, Campbell BA, et al. Understanding the lunar surface and space-Moon interactions. Reviews in Mineralogy and Geochemistry. 2006; **60**(1):83-219

[74] Vaniman D, Reedy R, Heiken G, Olhoeft G, Mendell W. The lunar environment. In: Heiken GH, Vaniman DT, French BM, editors. The Lunar Sourcebook: A User's Guide to the Moon. Cambridge: Cambridge University Press; 1991. pp. 27-60

[75] Ogilvie KW, Coplan MA. Solar wind composition. Reviews of Geophysics. 1995;**33**(S1):615-622

[76] Ryan JM, Lockwood JA, Debrunner H. Solar energetic particles. Space Science Reviews. 2000;**93**(1): 35-53

[77] Mewaldt RA. Solar energetic particle composition, energy spectra, and space weather. Space Science Reviews. 2006; **124**(1):303-316

[78] Garrard TL, Stone EC. Composition of energetic particles from solar flares. Advances in Space Research. 1994; **14**(10):589-598

[79] Farrell WM, Hurley DM, Esposito VJ, McLain JL, Zimmerman MI. The statistical mechanics of solar wind hydroxylation at the Moon, within lunar magnetic anomalies, and at Phobos. Journal of Geophysical Research: Planets. 2017; **122**(1):269-289

[80] Jones BM, Aleksandrov A, Hibbitts K, Dyar MD, Orlando TM. Solar wind-induced water cycle on the Moon. Geophysical Research Letters. 2018;**45**(20):10959-10967

[81] Tucker OJ, Farrell WM, Killen RM, Hurley DM. Solar wind implantation into the lunar Regolith: Monte Carlo simulations of H retention in a surface

with defects and the H2 exosphere. Journal of Geophysical Research: Planets. 2019;**124**(2):278-293

[82] Li S, Milliken RE. Water on the surface of the Moon as seen by the Moon mineralogy mapper: Distribution, abundance, and origins. Science Advances. 2017;**3**(9):e1701471

[83] Halekas JS, Delory GT, Lin RP, Stubbs TJ, Farrell WM. Lunar surface charging during solar energetic particle events: Measurement and prediction. Journal of Geophysical Research: Space Physics. 2009;**114**:A05110

[84] Halekas JS, Delory GT, Brain DA, Lin RP, Fillingim MO, Lee CO, et al. Extreme lunar surface charging during solar energetic particle events. Geophysical Research Letters. 2007;**34**: L02111

[85] Simpson JA. Elemental and isotopic composition of the galactic cosmic rays. Annual Review of Nuclear and Particle Science. 1983;**33**(1):323-382

[86] Heber B, Fichtner H, Scherer K. Solar and Heliospheric modulation of galactic cosmic rays. Space Science Reviews. 2006;**125**(1):81-93

[87] Mewaldt RA, Davis AJ, Lave KA, Leske RA, Stone EC, Wiedenbeck ME, et al. Record-setting cosmic-ray intensities in 2009 and 2010. The Astrophysical Journal. 2010;**723**(1): L1-L6

[88] Spence HE, Golightly MJ, Joyce CJ, Looper MD, Schwadron NA, Smith SS, et al. Relative contributions of galactic cosmic rays and lunar proton "albedo" to dose and dose rates near the Moon. Space Weather. 2013;**11**(11): 643-650

[89] Reitz G, Berger T, Matthiae D. Radiation exposure in the moon environment. Planetary and Space Science. 2012;**74**(1):78-83

[90] Naito M, Hasebe N, Shikishima M, Amano Y, Haruyama J, Matias-Lopes JA, et al. Radiation dose and its protection in the Moon from galactic cosmic rays and solar energetic particles: At the lunar surface and in a lava tube. Journal of Radiological Protection. 2020; **40**(4):947-961

[91] De Angelis G, Badavi FF, Clem JM, Blattnig SR, Clowdsley MS, Nealy JE, et al. Modeling of the lunar radiation environment. Nuclear Physics B—Proceedings Supplements. 2007;**166**: 169-183. Proceedings of the Third International Conference on Particle and Fundamental Physics in Space

[92] McMorrow D, Melinger JS, Knudson AR. Single-event effects in iii-v semiconductor electronics. International Journal of High Speed Electronics and Systems. 2004;**14**(02): 311-325

[93] Sexton FW. Destructive single-event effects in semiconductor devices and ICs. IEEE Transactions on Nuclear Science. 2003;**50**(3):603-621

[94] Stassinopoulos EG, Raymond JP. The space radiation environment for electronics. Proceedings of the IEEE. 1988;**76**(11):1423-1442

[95] Duzellier S. Radiation effects on electronic devices in space. Aerospace Science and Technology. 2005;**9**(1): 93-99

[96] Feynman J, Gabriel SB. On space weather consequences and predictions. Journal of Geophysical Research: Space Physics. 2000;**105**(A5):10543-10564

[97] Was GS. Fundamentals of radiation materials science: Metals and alloys. In: Chapter the Damage Cascade. New York, NY: Springer; 2017. pp. 131-165

[98] Zinkle SJ, Steven J. Radiation-induced effects on microstructure. In:

Comprehensive Nuclear Materials. Amsterdam: Elsevier; 2012. pp. 65-98

[99] Leonard KJ. 4.06 - radiation effects in refractory metals and alloys. In: Konings RJM, editor. Comprehensive Nuclear Materials. Oxford: Elsevier; 2012. pp. 181-213

[100] Ochoa M, Yaccuzzi E, Espinet-González P, Barrera M, Barrigín E, Ibarra ML, et al. 10MeV proton irradiation effects on GaInP/GaAs/Ge concentrator solar cells and their component subcells. Solar Energy Materials and Solar Cells. 2017;**159**:576-582

[101] Baur C, Gervasi M, Nieminen P, Pensotti S, Rancoita PG, Tacconi M. NIEL dose dependence for solar cells irradiated with electrons and protons. In: Proceedings of the 13th ICATPP Conference on Astroparticle, Particle, Space Physics and Detectors for Physics Applications. Singapore: World Scientific; 2013. pp. 692-707

[102] Kalos MH, Whitlock PA. Monte Carlo Methods Volume 1: Basics. New York: Wiley-Interscience Publication; 1986

[103] Cleri F. Monte-Carlo Methods for the Study of the Diffusion of Charged Particles through Matter. Singapore: World Scientific Publishing Co; 1990

[104] Fassò A, Ferrari A, Sala PR. Radiation transport calculations and simulations. Radiation Protection Dosimetry. 2009;**137**(1–2):118-133

[105] Allison J, Amako K, Apostolakis J, Araujo H, Arce Dubois P, Asai M, et al. Geant4 developments and applications. IEEE Transactions on Nuclear Science. 2006;**53**(1):270-278

[106] Werner CJ, editor. MCNP Users Manual—Code Version 6.2. Technical Report. Report LA-UR-17-29981. Los Alamos: Los Alamos National Security, LLC; 2018

[107] Werner CJ et al. MCNP6.2 Release Notes. Technical Report. Report LA-UR-18-20808. Los Alamos: Los Alamos National Laboratory; 2018

[108] Goorley T, James M, Booth T, Brown F, Bull J, Cox LJ, et al. Initial MCNP6 release overview. Nuclear Technology. 2012;**180**(3):298-315

[109] Battistoni G. The FLUKA code, galactic cosmic ray and solar energetic particle events: From fundamental physics to space radiation and commercial aircraft doses. In: 2008 IEEE Nuclear Science Symposium Conference Record. Piscataway, NJ: IEEE; 2008. pp. 1609-1615

[110] Sato T, Niita K, Matsuda N, Hashimoto S, Iwamoto Y, Noda S, et al. Particle and Heavy Ion Transport code System, PHITS, version 2.52. Journal of Nuclear Science and Technology. 2013; **50**(9):913-923

[111] Townsend LW, Miller TM, Gabriel TA. HETC radiation transport code development for cosmic ray shielding applications in space. Radiation Protection Dosimetry. 2005; **116**(1–4 Pt 2):135-139

[112] Jia Y, Lin ZW. The radiation environment on the moon from galactic cosmic rays in a lunar habitat. Radiation Research. 2010;**173**(2):238-244

[113] Pham TT, El-Genk MS. Simulations of space radiation interactions with materials and dose estimates for a lunar shelter and aboard the international space station. In: Technical report, Institute for Space and Nuclear Power Studies (ISNPS). Technical Report ISNPS-UNM-1-2013. Albuquerque, NM: University of New Mexico; 2013

[114] Zaman FA, Townsend LW, de Wet WC, Burahmah NT. The lunar radiation environment: Comparisons between PHITS, HETC-HEDS, and the

CRaTER instrument. Aerospace. 2021; **8**(7):182

[115] Spence H, Case A, Golightly M, Heine T, Larsen B, Blake J, et al. CRaTER: The cosmic ray telescope for the effects of radiation experiment on the lunar reconnaissance orbiter mission. Space Science Reviews. 2010;**150**:243-284

[116] Lindhard J, Winther A. Stopping power of electron gas and equipartition rule. Det Kongelige Danske Videnskabernes Selskab. Matematisk-fysiske Meddelelser. 1964;**34**(4):1

[117] Koval NE, Da Pieve F, Artacho E. *Ab initio* electronic stopping power for protons in $Ga_{0.5}In_{0.5}P$/GaAs/Ge triple-junction solar cells for space applications. Royal Society Open Science. 2020;**7**(11):200925

[118] Lee C-W, Stewart JA, Dingreville R, Foiles SM, Schleife A. Multiscale simulations of electron and ion dynamics in self-irradiated silicon. Physical Review B. 2020;**102**:024107

[119] Smith R. Atomic and Ion Collisions in Solids and at Surfaces: Theory, Simulation and Applications. Cambridge: Cambridge University Press; 1997

[120] Ziegler JF, Ziegler MD, Biersack JP. SRIM—The stopping and range of ions in matter. NIMB. 2010;**268**(11):1818-1823

[121] Nordlund K, Djurabekova F. Multiscale modelling of irradiation in nanostructures. Journal of Computational Electronics. 2014;**13**(1): 122-141

[122] Apostolova T, Artacho E, Cleri F, Cotelo M, Crespillo ML, Da Pieve F, et al. Fundamentals of Monte Carlo Particle Transport and Synergies with Quantum Dynamics for Applications in Ion-irradiated Materials in Space and Radiobiology. In: Tools for investigating electronic excitation: Experiment and multiscale modelling. Instituto de Fusión Nuclear "Guillermo Velarde", Universidad Politécnica de Madrid; 2021. pp. 345-374

[123] Marques MAL, Maitra NT, Nogueira FMS, Gross EKU, Rubio A. Fundamentals of Time-Dependent Density Functional Theory. Berlin: Springer; 2012

[124] Iftimie R, Minary P, Tuckerman ME. Ab initio molecular dynamics: Concepts, recent developments, and future trends. Proceedings of the National Academy of Sciences. 2005;**102**(19):6654-6659

[125] Hohenberg P, Kohn W. Inhomogeneous electron gas. Physics Review. 1964;**136**:B864-B871

[126] Kohn W, Sham LJ. Self-consistent equations including exchange and correlation effects. Physics Review. 1965;**140**:A1133-A1138

[127] Gillespie DT. A general method for numerically simulating the stochastic time evolution of coupled chemical reactions. Journal of Computational Physics. 1976;**22**(4):403-434

[128] Ghoniem NM, Cui Y. 1.22—Dislocation dynamics simulations of defects in irradiated materials. In: Konings RJM, Stoller RE, editors. Comprehensive Nuclear Materials. 2nd ed. Oxford: Elsevier; 2020. pp. 689-716

[129] Clough RW. The finite element method in plane stress analysis. In: Proceedings of 2nd ASCE Conference on Electronic Computation; Sept. 8 and 9, 1960. Pittsburgh, Pa: American Society of Civil Engineers; 1960

[130] Marian J, Becquart CS, Domain C, Dudarev SL, Gilbert MR, Kurtz RJ, et al. Recent advances in modeling and simulation of the exposure and response

of tungsten to fusion energy conditions. Nuclear Fusion. 2017;**57**(9):092008

[131] Bacon DJ, Osetsky YN. Multiscale modelling of radiation damage in metals: From defect generation to material properties. Materials Science and Engineering A, Structural Materials: Properties, Microstructure and Processing. 2004;**365**(1–2):46-56

[132] Chen D, He X, Chu G, He X, Jia L, Wang Z, et al. An overview: Multiscale simulation in understanding the radiation damage accumulation of reactor materials. Simulation. 2021; **97**(10):659-675

[133] Holm A, Mayr SG. Glassy and ballistic dynamics in collision cascades in amorphous TiO_2: Combined molecular dynamics and Monte Carlo based studies across energy scales. Physical Review B. 2021;**103**:174201

[134] Raine M, Jay A, Richard N, Goiffon V, Girard S, Gaillardin M, et al. Simulation of single particle displacement damage in silicon—Part I: Global approach and primary interaction simulation. IEEE Transactions on Nuclear Science. 2017; **64**(1):133-140

[135] Bacon DJ, Diaz de la Rubia T. Molecular dynamics computer simulations of displacement cascades in metals. Journal of Nuclear Materials. 1994;**216**:275-290

[136] Foiles SM, Baskes MI, Daw MS. Embedded-atom-method functions for the fcc metals Cu, Ag, Au, Ni, Pd, Pt, and their alloys. Physical Review B. 1986;**33**:7983-7991

[137] Malerba L, Marinica MC, Anento N, Björkas C, Nguyen H, Domain C, et al. Comparison of empirical interatomic potentials for iron applied to radiation damage studies. Journal of Nuclear Materials. 2010; **406**(1):19-38. FP6 IP PERFECT Project: Prediction of Irradiation Damage Effects in Reactor Components

[138] Brommer P, Kiselev A, Schopf D, Beck P, Roth J, Trebin H-R. Classical interaction potentials for diverse materials from ab initio data: A review of potfit. Modelling and Simulation in Materials Science and Engineering. 2015;**23**(7):074002

[139] Nordlund K. Historical review of computer simulation of radiation effects in materials. Journal of Nuclear Materials. 2019;**520**:273-295

[140] Allen MP, Tildesley DJ. Computer Simulation of Liquids. Oxford: Oxford University Press; 2017

[141] Frenkel D, Smit B. Understanding Molecular Simulation: From Algorithms to Applications. Amsterdam: Elsevier; 2001

[142] Nordlund K, Wallenius J, Malerba L. Molecular dynamics simulations of threshold displacement energies in Fe. Nuclear Instruments and Methods in Physics Research Section B: Beam Interactions with Materials and Atoms. 2006;**246**(2):322-332

[143] Sand AE, Dudarev SL, Nordlund K. High-energy collision cascades in tungsten: Dislocation loops structure and clustering scaling laws. EPL (Europhysics Letters). 2013;**103**(4): 46003

[144] Van Brutzel L, Crocombette JP. Classical molecular dynamics study of primary damage created by collision cascade in a ZrC matrix. Nuclear instruments and methods in physics research section B: Beam interactions with materials and atoms. 2007;**255**(1): 141-145. Computer Simulation of Radiation Effects in Solids

[145] Bonny G, Buongiorno L, Bakaev A, Castin N. Models and regressions to describe primary damage in silicon

carbide. Scientific Reports. 2020;**10**(1): 10483

[146] Martin G, Garcia P, Van Brutzel L, Dorado B, Maillard S. Effect of the cascade energy on defect production in uranium dioxide. Nuclear Instruments and Methods in Physics Research Section B: Beam Interactions with Materials and Atoms. 2011;**269**(14): 1727-1730. Computer Simulations of Radiation Effects in Solids

[147] Amini M, Azadegan B, Akbarzadeh H, Gharaei R. Analysis of MoS2 and WS2 nano-layers role on the radiation resistance of various Cu/MS2/Cu and Cu/MS2@Cu@MS2/Cu nanocomposites. Materialia. 2021;**21**: 101281

[148] Shi T, Peng Q, Bai Z, Gao F, Jovanovic I. Proton irradiation of graphene: Insights from atomistic modeling. Nanoscale. 2019;**11**: 20754-20765

[149] Zhang Y, Zhao S, Weber WJ, Nordlund K, Granberg F, Djurabekova F. Atomic-level heterogeneity and defect dynamics in concentrated solid-solution alloys. Current Opinion in Solid State and Materials Science. 2017;**21**(5):221-237. Concentrated Solid Solution Alloys Perspective

[150] Granberg F, Nordlund K, Ullah MW, Jin K, Lu C, Bei H, et al. Mechanism of radiation damage reduction in equiatomic multicomponent single phase alloys. Physical Review Letters. 2016;**116**: 135504

[151] Yang YI, Shao Q, Zhang J, Yang L, Gao YQ. Enhanced sampling in molecular dynamics. The Journal of Chemical Physics. 2019;**151**(7): 070902

[152] Voter AF. Introduction to the kinetic Monte Carlo method. In: Sickafus KE, Kotomin EA, Uberuaga BP, editors. Radiation Effects in Solids. Netherlands, Dordrecht: Springer; 2007. pp. 1-23

[153] Caturla MJ. Object kinetic Monte Carlo methods applied to modeling radiation effects in materials. Computational Materials Science. 2019; **156**:452-459

[154] Gao Y, Zhang Y, Schwen D, Jiang C, Sun C, Gan J, et al. Theoretical prediction and atomic kinetic Monte Carlo simulations of void superlattice self-organization under irradiation. Scientific Reports. 2018;**8**(1):6629

[155] Soisson F. Kinetic Monte Carlo simulations of radiation induced segregation and precipitation. Journal of Nuclear Materials. 2006;**349**(3):235-250

[156] Bathe K-J. Finite Element Method. In: Wiley encyclopedia of computer science and engineering. Hoboken, NJ: John Wiley & Sons, Ltd; 2008. pp. 1-12

[157] Marx D, Hutter J. Ab Initio Molecular Dynamics: Basic Theory and Advanced Methods. Cambridge: Cambridge University Press; 2009

[158] Born M, Oppenheimer R. Zur Quantentheorie der Molekeln. Annalen der Physik. 1927;**389**(20):457-484

[159] Parr RG, Weitao Y. Density-Functional Theory of Atoms and Molecules. International Series of Monographs on Chemistry. Oxford: Oxford University Press; 1994

[160] Runge E, Gross EKU. Density-functional theory for time-dependent systems. Physical Review Letters. 1984; **52**:997-1000

[161] Ehrenfest P. Bemerkung über die angenäherte gültigkeit der klassischen mechanik innerhalb der quantenmechanik. Zeitschrift für Physik. 1927;**45**(7):455-457

[162] Tully JC. Molecular dynamics with electronic transitions. The Journal of Chemical Physics. 1990;**93**(2):1061-1071

[163] Correa AA, Kohanoff J, Artacho E, Sánchez-Portal D, Caro A. Nonadiabatic forces in ion-solid interactions: The initial stages of radiation damage. Physical Review Letters. 2012;**108**: 213201

[164] Ahsan Zeb M, Kohanoff J, Sánchez-Portal D, Arnau A, Juaristi JI, Artacho E. Electronic stopping power in gold: The role of *d* electrons and the H/He anomaly. Physical Review Letters. 2012;**108**:225504

[165] Quijada M, Borisov AG, Nagy I, Dez Muiño R, Echenique PM. Time-dependent density-functional calculation of the stopping power for protons and antiprotons in metals. Physical Review A. 2007;**75**:042902

[166] Koval NE, Borisov AG, Rosa LFS, Stori EM, Dias JF, Grande PL, et al. Vicinage effect in the energy loss of H_2 dimers: Experiment and calculations based on time-dependent density-functional theory. Physical Review A. 2017;**95**:062707

[167] Yost DC, Yao Y, Kanai Y. Examining real-time time-dependent density functional theory nonequilibrium simulations for the calculation of electronic stopping power. Physical Review B. 2017;**96**:115134

[168] Maliyov I, Crocombette J-P, Bruneval F. Electronic stopping power from time-dependent density-functional theory in gaussian basis. The European Physical Journal B. 2018; **91**(8):172

[169] Duffy DM, Rutherford AM. Including the effects of electronic stopping and electron–ion interactions in radiation damage simulations. Journal of Physics: Condensed Matter. 2006; **19**(1):016207

[170] Tamm A, Caro M, Caro A, Samolyuk G, Klintenberg M, Correa AA. Langevin dynamics with spatial correlations as a model for Electron-phonon coupling. Physical Review Letters. 2018;**120**:185501

[171] Jarrin T, Richard N, Teunissen J, Da Pieve F, Hémeryck A. Integration of electronic effects into molecular dynamics simulations of collision cascades in silicon from first-principles calculations. Physical Review B. 2021; **104**:195203

[172] Darkins R, Duffy DM. Modelling radiation effects in solids with two-temperature molecular dynamics. Computational Materials Science. 2018; **147**:145-153

[173] Caro M, Tamm A, Correa AA, Caro A. Role of electrons in collision cascades in solids. I. Dissipative model. Physical Review B. 2019;**99**:174301

[174] Tamm A, Caro M, Caro A, Correa AA. Role of electrons in collision cascades in solids. II. Molecular dynamics. Physical Review B. 2019;**99**:174302

[175] Akkerman A, Barak J, Chadwick MB, Levinson J, Murat M, Lifshitz Y. Updated NIEL calculations for estimating the damage induced by particles and γ-rays in Si and GaAs. Radiation Physics and Chemistry. 2001; **62**(4):301-310

[176] Moll M. Displacement damage in silicon detectors for high energy physics. IEEE Transactions on Nuclear Science. 2018;**65**(8):1561-1582

[177] Dawson I, Faccio F, Moll M, Weidberg A. Radiation Effects in the LHC Experiments: Impact on Detector Performance and Operation. Technical Report. Report CERN-2021-001. Geneva: CERN; 2021

[178] Srour JR. Review of displacement damage effects in silicon devices. IEEE

Transactions on Nuclear Science. 2003; **50**(3):653-670

[179] Srour JR, Lo DH. Universal damage factor for radiation-induced dark current in silicon devices. IEEE Transactions on Nuclear Science. 2000; **47**(6):2451-2459

[180] Summers GP, Burke EA, Shapiro P, Messenger SR, Walters R. Damage correlation in semiconductors exposed to gamma, electron and proton radiations. IEEE Transactions on Nuclear Science. 1993;**40**(6):1372-1379

[181] Messenger SR, Summers GP, Burke EA, Walters RJ, Xapsos MA. Modeling solar cell degradation in space: A comparison of the NRL displacement damage dose and the JPL equivalent fluence approaches. Progress in Photovoltaics: Research and Applications. 2001;**9**(2):103-121

[182] Summers GP, Walters RJ, Xapsos MA, Burke EA, Messenger SR, Shapiro P, et al. A new approach to damage prediction for solar cells exposed to different radiations. In: IEEE Proceedings of 1st World Conference on Photovoltaic Energy Conversion, Waikoloa, HI. 1994. Piscataway, NJ: IEEE; 1994. pp. 2068-2073

[183] Moll M, Fretwurst E, Kuhnke M, Lindstroem G. Relation between microscopic defects and macroscopic changes in silicon detector properties after hadron irradiation. Nuclear Instruments and Methods in Physics Research Section B: Beam Interactions with Materials and Atoms. 2002;**186**:100-110

[184] Norgett MJ, Robinson MT, Torrens IM. A proposed method of calculating displacement dose rates. Nuclear Engineering and Design. 1975; **33**(1):50-54

[185] Okuno Y, Okuda S, Akiyoshi M, Oka T, Harumoto M, Omura K, et al. Radiation degradation prediction for InGaP solar cells by using appropriate estimation method for displacement threshold energy. Journal of Applied Physics. 2017;**122**(11):114901

[186] Salzberger M, Nömayr C, Lugli P, Messenger SR, Zimmermann CG. Degradation fitting of irradiated solar cells using variable threshold energy for atomic displacement. Progress in Photovoltaics: Research and Applications. 2017;**25**(9):773-781

[187] Holmström E, Nordlund K, Kuronen A. Threshold defect production in germanium determined by density functional theory molecular dynamics simulations. Physica Scripta. 2010;**81**(3):035601

[188] Jiang M, Xiao H, Peng S, Yang G, Liu Z, Qiao L, et al. A theoretical simulation of the radiation responses of Si, Ge, and Si/Ge superlattice to low-energy irradiation. Nanoscale Research Letters. 2018;**13**(1):133

[189] Okuno Y, Ishikawa N, Akiyoshi M, Ando H, Harumoto M, Imaizumi M. Degradation prediction using displacement damage dose method for AlInGaP solar cells by changing displacement threshold energy under irradiation with low-energy electrons. Japanese Journal of Applied Physics. 2020;**59**(7):074001

[190] Boschini MJ, Rancoita PG, Tacconi M. SR-NIEL Calculator: Screened Relativistic (SR) Treatment for Calculating the Displacement Damage and Nuclear Stopping Powers for Electrons, Protons, Light- and Heavy- Ions in Materials (version 7.7.0). 2014. Available from: http://www.sr-niel.org/ [Accessed: December 17, 2021]

[191] Radu R, Pintilie I, Nistor LC, Fretwurst E, Lindstroem G, Makarenko LF. Investigation of point and extended defects in electron irradiated silicon–dependence on the

particle energy. Journal of Applied Physics. 2015;**117**(16):164503

[192] Inguimbert C, Arnolda P, Nuns T, Rolland G. "Effective NIEL" in silicon: Calculation using molecular dynamics simulation results. IEEE Transactions on Nuclear Science. 2010;**57**(4):1915-1923

[193] Inguimbert C, Messenger S. Equivalent displacement damage dose for on-orbit space applications. IEEE Transactions on Nuclear Science. 2012; **59**(6):3117-3125

[194] Gao F, Chen N, Hernandez-Rivera E, Huang D, LeVan PD. Displacement damage and predicted non-ionizing energy loss in GaAs. Journal of Applied Physics. 2017;**121**(9):095104

[195] Messenger SR, Jackson EM, Warner JH, Walters RJ, Cayton TE, Chen Y, et al. Correlation of telemetered solar Array data with particle detector data on GPS spacecraft. IEEE Transactions on Nuclear Science. 2011; **58**(6):3118-3125

[196] Lu MX, Wang RC, Liu YH, Hu WT, Feng Z, Han Z. Adjusted NIEL calculations for estimating proton-induced degradation of GaInP/GaAs/Ge space solar cells. Nuclear Instruments & Methods in Physics Research Section B-beam Interactions With Materials and Atoms. 2011;**269**:1884-1886

[197] Nordlund K, Zinkle SJ, Sand AE, Granberg F, Averback RS, Stoller R, et al. Improving atomic displacement and replacement calculations with physically realistic damage models. Nature Communications. 2018;**9**(1):1084

[198] Crocombette J-P, Wambeke V, Christian. Quick calculation of damage for ion irradiation: Implementation in Iradina and comparisons to SRIM. EPJ Nuclear Science and Technology. 2019;**5**:7

[199] Jarrin T, Jay A, Hémeryck A, Richard N. Parametric study of the two-temperature model for molecular dynamics simulations of collisions cascades in Si and Ge. Nuclear Instruments and Methods in Physics Research Section B: Beam Interactions with Materials and Atoms. 2020;**485**:1-9

[200] Li W, Stroppa A, Wang Z-M, Gao S. Hybrid Organic-Inorganic Perovskites, Chapter 1. Weinheim, Germany: Wiley-VCH Verlag GmbH & Co. KGaA; 2020

[201] Eames C, Frost JM, Barnes PRF, O'Regan BC, Walsh A, Islam MS. Ionic transport in hybrid lead iodide perovskite solar cells. Nature Communications. 2015;**6**(1):7497

[202] Boyd CC, Cheacharoen R, Leijtens T, McGehee MD. Understanding degradation mechanisms and improving stability of perovskite photovoltaics. Chemical Reviews. 2019; **119**(5):3418-3451

[203] Zhang Y-Y, Chen S, Peng X, Xiang H, Gong X-G, Walsh A, et al. Intrinsic instability of the hybrid halide perovskite semiconductor CH3NH3PbI3*. Chinese Physics Letters. 2018;**35**(3):036104

[204] Akbulatov AF, Frolova LA, Dremova NN, Zhidkov I, Martynenko VM, Tsarev SA, et al. Light or heat: What is killing lead halide perovskites under solar cell operation conditions? The Journal of Physical Chemistry Letters. 2020;**11**(1): 333-339

[205] Ava T, Mamun A, Marsillac S, Namkoong G. A review: Thermal stability of methylammonium lead halide based perovskite solar cells. Applied Sciences. 2019;**9**:188

[206] Niu G, Guo X, Wang L. Review of recent progress in chemical stability of perovskite solar cells. Journal of Materials Chemistry A. 2015;**3**: 8970-8980

[207] Meggiolaro D, Motti SG, Mosconi E, Barker AJ, Ball J, Perini CAR, et al. Iodine chemistry determines the defect tolerance of lead-halide perovskites. Energy & Environmental Science. 2018;**11**:702-713

[208] Oranskaia A, Schwingenschlögl U. Suppressing X-migrations and enhancing the phase stability of cubic FAPbX3 (X = Br, I). Advanced Energy Materials. 2019;**9**(32):1901411

[209] Futscher MH, Lee JM, McGovern L, Muscarella LA, Wang T, Haider MI, et al. Quantification of ion migration in CH3NH3PbI3 perovskite solar cells by transient capacitance measurements. Materials Horizons. 2019;**6**:1497-1503

[210] Khan R, Ighodalo KO, Xiao Z. Ion Migration in Metal Halide Perovskites Solar Cells. In: Soft-Matter Thin Film Solar Cells. Melville, New York: AIP Publishing LLC.; 2020

[211] Lang F, Shargaieva O, Brus VV, Neitzert HC, Rappich J, Nickel NH. Influence of radiation on the properties and the stability of hybrid perovskites. Advanced Materials. 2018;**30**(3): 1702905

[212] McMillon-Brown L, Crowley KM, VanSant KT, Peshek TJ. Prospects for perovskites in space. In: Proceedings of 2021 IEEE 48th Photovoltaic Specialists Conference (PVSC). Piscataway, NJ: IEEE; 2021. pp. 0222-0225

[213] Wu S, Li Z, Li M-Q, Diao Y, Lin F, Liu T, et al. 2d metal–organic framework for stable perovskite solar cells with minimized lead leakage. Nature Nanotechnology. 2020;**15**(11): 934-940

[214] Wolf MJ, Ghosh D, Kullgren J, Pazoki M. Characterizing MAPbI3 with the aid of first principles calculations. In: Pazoki M, Hagfeldt A, Edvinsson T, editors. Characterization Techniques for Perovskite Solar Cell Materials, Micro and Nano Technologies. Amsterdam: Elsevier; 2020. pp. 217-236

[215] Teunissen JL, Da Pieve F. Molecular bond engineering and feature learning for the design of hybrid organic-inorganic perovskite solar cells with strong noncovalent halogen–cation interactions. Journal of Physical Chemistry C. 2021;**45**:45

[216] Reb LK, Böhmer M, Predeschly B, Grott S, Weindl CL, Ivandekic GI, et al. Perovskite and organic solar cells on a rocket flight. Joule. 2020;**4**(9): 1880-1892

[217] Lang F, Jošt M, Frohna K, Köhnen E, Al-Ashouri A, Bowman AR, et al. Proton radiation hardness of perovskite tandem photovoltaics. Joule; **4**(5):1054-1069

[218] Malinkiewicz O, Imaizumi M, Sapkota SB, Ohshima T, Öz S. Radiation effects on the performance of flexible perovskite solar cells for space applications. Emergent Materials. 2020; **3**(1):9-14

[219] Kanaya S, Kim GM, Ikegami M, Miyasaka T, Suzuki K, Miyazawa Y, et al. Proton irradiation tolerance of high-efficiency perovskite absorbers for space applications. The Journal of Physical Chemistry Letters. 2019; **10**(22):6990-6995

[220] Shin J, Baek K-Y, Lee J, Lee W, Kim J, Jang J, et al. Proton irradiation effects on mechanochemically synthesized and flash-evaporated hybrid organic–inorganic lead halide perovskites. Nanotechnology. 2021; **33**(6):065706

[221] Cai Z, Yuning W, Chen S. Energy-dependent knock-on damage of organic–inorganic hybrid perovskites under electron beam irradiation: First-principles insights. Applied Physics Letters. 2021;**119**(12):123901

[222] Tsai M-H, Yeh J-W. High-entropy alloys: A critical review. Materials Research Letters. 2014;**2**(3):107-123

[223] Senkov ON, Miller JD, Miracle DB, Woodward C. Accelerated exploration of multi-principal element alloys with solid solution phases. Nature Communications. 2015;**6**:6529

[224] Fan Z, Tong Y, Zhang Y. High-entropy materials: Theory, experiments, and applications. In: Chapter Radiation Damage in Concentrated Solid-Solution and High-Entropy Alloys. Cham: Springer International Publishing; 2021. pp. 645-685

[225] Wang S. Atomic structure modeling of multi-principal-element alloys by the principle of maximum entropy. Entropy. 2013;**15**(12):5536-5548

[226] Sathiyamoorthi P, Kim H. High-entropy alloys: Potential candidates for high-temperature applications—An overview. Advanced Engineering Materials. 2017;**20**:10

[227] Yan X, Zhang Y. Functional properties and promising applications of high entropy alloys. Scripta Materialia. 2020;**187**:188-193

[228] Ye YF, Wang Q, Lu J, Liu CT, Yang Y. High-entropy alloy: Challenges and prospects. Materials Today. 2016; **19**(6):349-362

[229] Kivy MB, Hong Y, Zaeem MA. A review of multi-scale computational modeling tools for predicting structures and properties of multi-principal element alloys. Metals. 2019;**9**(2):254

[230] Shang Y, Brechtl J, Psitidda C, Liaw PK. Mechanical behavior of high-entropy alloys: A review, 2021. arXiv preprint 2102.09055

[231] Chen W-Y, Liu X, Chen Y, Yeh J-W, Tseng K-K, Natesan K. Irradiation effects in high entropy alloys and 316H stainless steel at 300°C. Journal of Nuclear Materials. 2018;**510**:421-430

[232] Pickering EJ, Carruthers AW, Barron PJ, Middleburgh SC, Armstrong DEJ, Gandy AS. High-entropy alloys for advanced nuclear applications. Entropy. 2021;**23**(1):98

[233] Lin Y, Yang T, Lang L, Shan C, Deng H, Wangyu H, et al. Enhanced radiation tolerance of the Ni-Co-Cr-Fe high-entropy alloy as revealed from primary damage. Acta Materialia. 2020; **196**:133-143

[234] Han C, Fang Q, Shi Y, Tor S, Chua K, Zhou K. Recent advances on high-entropy alloys for 3D printing. Advanced Materials. 2020;**32**:1903855

[235] Egami T, Guo W, Rack PD, Nagase T. Irradiation resistance of multicomponent alloys. Metallurgical and Materials Transactions A. 2014; **45**(1):180-183

[236] Xia S-q, Wang Z, Yang T-f, Zhang Y. Irradiation behavior in high entropy alloys. Journal of Iron and Steel Research International. 2015;**22**(10): 879-884

[237] Nagase T, Anada S, Rack PD, Noh JH, Yasuda H, Mori H, et al. MeV electron-irradiation-induced structural change in the bcc phase of Zr-Hf-Nb alloy with an approximately equiatomic ratio. Intermetallics. 2013;**38**:70-79

[238] Patel D, Richardson MD, Jim B, Akhmadaliev S, Goodall R, Gandy AS. Radiation damage tolerance of a novel metastable refractory high entropy alloy V2.5Cr1.2WMoCo0.04. Journal of Nuclear Materials. 2020;**531**:152005

[239] Shao L, Zhang T, Li L, Zhao Y, Huang J, Liaw PK, et al. A low-cost lightweight entropic alloy with high strength. Journal of Materials Engineering and Performance. 2018;**27**(12):6648-6656

[240] Feng R, Gao MC, Lee C, Mathes M, Zuo T, Chen S, et al. Design of light-weight high-entropy alloys. Entropy. 2016;**18**(9):333

[241] Maulik O, Kumar D, Kumar S, Dewangan SK, Kumar V. Structure and properties of lightweight high entropy alloys: A brief review. Materials Research Express. 2018;**5**(5):052001

[242] Taylor SR. Lunar Science: A Post-Apollo View; Scientific Results and Insights from the Lunar Samples. New York: Pergamon Press; 1975

[243] Aizenshtein M, Ungarish Z, Woller KB, Hayun S, Short MP. Mechanical and microstructural response of the Al0.5CoCrFeNi high entropy alloy to Si and Ni ion irradiation. Nuclear Materials and Energy. 2020;**25**:100813

[244] Lu C, Niu L, Chen N, Jin K, Yang T, Xiu P, et al. Enhancing radiation tolerance by controlling defect mobility and migration pathways in multicomponent single-phase alloys. Nature Communications. 2016;**7**(1):13564

[245] Do H-S, Lee B-J. Origin of radiation resistance in multi-principal element alloys. Scientific Reports. 2018;**8**(1): 16015

[246] Nordlund K, Zinkle SJ, Sand AE, Granberg F, Averback RS, Stoller RE, et al. Primary radiation damage: A review of current understanding and models. Journal of Nuclear Materials. 2018;**512**:450-479

[247] Li Y, Li R, Peng Q, Ogata S. Reduction of dislocation, mean free path, and migration barriers using high entropy alloy: Insights from the atomistic study of irradiation damage of CoNiCrFeMn. Nanotechnology. 2020; **31**(42):425701

[248] Zhang Y, Stocks GM, Jin K, Lu C, Bei H, Sales BC, et al. Influence of chemical disorder on energy dissipation and defect evolution in concentrated solid solution alloys. Nature Communications. 2015;**6**(1):8736

[249] Quashie EE, Ullah R, Andrade X, Correa AA. Effect of chemical disorder on the electronic stopping of solid solution alloys. Acta Materialia. 2020; **196**:576-583

[250] Zarkadoula E, Samolyuk G, Weber WJ. Effects of electronic excitation on cascade dynamics in nickel–iron and nickel–palladium systems. Scripta Materialia. 2017;**138**: 124-129

[251] Zarkadoula E, Samolyuk G, Weber WJ. Effects of electron-phonon coupling and electronic thermal conductivity in high energy molecular dynamics simulations of irradiation cascades in nickel. Computational Materials Science. 2019;**162**:156-161

[252] Zarkadoula E, Samolyuk G, Weber WJ. Two-temperature model in molecular dynamics simulations of cascades in Ni-based alloys. Journal of Alloys and Compounds. 2017;**700**:106-112

[253] Zarkadoula E, Samolyuk G, Weber WJ. Effects of electronic excitation in 150 keV Ni ion irradiation of metallic systems. AIP Advances. 2018;**8**(1):015121

[254] Zarkadoula E, Samolyuk G, Xue H, Bei H, Weber WJ. Effects of two-temperature model on cascade evolution in Ni and NiFe. Scripta Materialia. 2016; **124**:6-10

[255] Biswas K, Yeh J-W, Bhattacharjee PP, DeHosson JTHM. High entropy alloys: Key issues under passionate debate. Scripta Materialia. 2020;**188**:54-58

[256] Béland LK, Lu C, Osetskiy YN, Samolyuk GD, Caro A, Wang L, et al. Features of primary damage by high energy displacement cascades in

concentrated Ni-based alloys. Journal of Applied Physics. 2016;**119**(8):085901

[257] Westermayr J, Gastegger M, Schütt KT, Maurer RJ. Perspective on integrating machine learning into computational chemistry and materials science. The Journal of Chemical Physics. 2021;**154**(23):230903

[258] Schmidt J, Marques MRG, Botti S, Marques MAL. Recent advances and applications of machine learning in solid-state materials science. npj Computational Materials. 2019;**5**(1):83

[259] Anatole von Lilienfeld O, Müller K-R, Tkatchenko A. Exploring chemical compound space with quantum-based machine learning. Nature Reviews Chemistry. 2020;**4**(7):347-358

[260] Behler J. Perspective: Machine learning potentials for atomistic simulations. The Journal of Chemical Physics. 2016;**145**(17):170901

[261] Wang H, Guo X, Zhang L, Wang H, Xue J. Deep learning inter-atomic potential model for accurate irradiation damage simulations. Applied Physics Letters. 2019;**114**(24):244101

[262] Morawietz T, Artrith N. Machine learning-accelerated quantum mechanics-based atomistic simulations for industrial applications. Journal of Computer-Aided Molecular Design. 2021;**35**(4):557-586

[263] Alexander R, Proville L, Becquart CS, Goryeava AM, Dérès J, Lapointe C, et al. Interatomic potentials for irradiation-induced defects in iron. Journal of Nuclear Materials. 2020;**535**: 152141

[264] Dragoni D, Daff TD, Csányi G, Marzari N. Achieving DFT accuracy with a machine-learning interatomic potential: Thermomechanics and defects in bcc ferromagnetic iron. Physical Review Materials. 2018;**2**:013808

[265] Byggmästar J, Hamedani A, Nordlund K, Djurabekova F. Machine-learning interatomic potential for radiation damage and defects in tungsten. Physical Review B. 2019;**100**: 144105

[266] Rosenbrock CW, Gubaev K, Shapeev AV, Pártay LB, Bernstein N, Csányi G, et al. Machine-learned interatomic potentials for alloys and alloy phase diagrams. npj Computational Materials. 2021;**7**(1):24

[267] Jafary-Zadeh M, Khoo KH, Laskowski R, Branicio PS, Shapeev AV. Applying a machine learning interatomic potential to unravel the effects of local lattice distortion on the elastic properties of multi-principal element alloys. Journal of Alloys and Compounds. 2019;**803**:1054-1062

[268] Singh R, Singh P, Sharma A, Bingol OR, Balu A, Balasubramanian G, et al. Neural-network model for force prediction in multi-principal-element alloys. Computational Materials Science. 2021;**198**:110693

[269] Singh R, Sharma A, Singh P, Balasubramanian G, Johnson DD. Accelerating computational modeling and design of high-entropy alloys. Nature Computational Science. 2021; **1**(1):54-61

[270] Yan Y, Dan L, Wang K. Accelerated discovery of single-phase refractory high entropy alloys assisted by machine learning. Computational Materials Science. 2021;**199**:110723

[271] Behler J, Parrinello M. Generalized neural-network representation of high-dimensional potential-energy surfaces. Physical Review Letters. 2007;**98**:146401

[272] Castin N, Pascuet MI, Messina L, Domain C, Olsson P, Pasianot RC, et al. Advanced atomistic models for radiation damage in fe-based alloys: Contributions and future perspectives

from artificial neural networks. Computational Materials Science. 2018; **148**:116-130

[273] Byggmästar J, Nordlund K, Djurabekova F. Modeling refractory high-entropy alloys with efficient machine-learned interatomic potentials: Defects and segregation. Physical Review B. 2021;**104**:104101

[274] Masuelli MA. Introduction of fibre-reinforced polymers- polymers and composites: Concepts, properties and processes. In: Fiber Reinforced Polymers —The Technology Applied for Concrete Repair. London, UK: IntechOpen; 2013

[275] Chabert E, Vial J, Cauchois J-P, Mihaluta M, Tournilhac F. Multiple welding of long fiber epoxy vitrimer composites. Soft Matter. 2016;**12**: 4838-4845

[276] Rojdev K, O'Rourke MJE, Hill C, Nutt S, Atwell W. Radiation effects on composites for long-duration lunar habitats. Journal of Composite Materials. 2014;**48**(7):861-878

[277] Tucker D, Ethridge E, and Toutanji H. Production of Glass Fibers for Reinforcement of Lunar Concrete. In: Proceedings of the 44th AIAA Aerospace Sciences Meeting and Exhibit. Nevada, Reno. US: NTRS; 2006 Cham, Switzerland: Springer; 2019

[278] Kumar V, Chaudhary B, Sharma V, Verma K. Radiation Effects in Polymeric Materials. Springer; 2019

[279] Jawaid M, Thariq M, Saba N. Mechanical and Physical Testing of Biocomposites, Fibre-Reinforced Composites and Hybrid Composites. Kidlington, UK: Woodhead Publishing; 2018

[280] Syamsir A, Ishak ZAM, Yusof ZM, Salwi N, Nadhirah A. Durability control of UV radiation in glass fiber reinforced polymer (GFRP)—A review. AIP Conference Proceedings. 2018;**2031**: 020033

[281] Kudoh H, Kasai N, Sasuga T, Seguchi T. Low temperature gamma-ray irradiation effects of polymer materials on mechanical property. Radiation Physics and Chemistry. 1994;**43**(4):329-334

[282] Idesaki A, Uechi H, Hakura Y, Kishi H. Effects of gamma-ray irradiation on a cyanate ester/epoxy resin. Radiation Physics and Chemistry. 2014;**98**:1-6

[283] Sonoda K, Enomoto J, Nakazaki K, Murayama K. Space radiation effects on mechanical properties of carbon fibre reinforced plastic. Japanese Journal of Applied Physics. 1988;**27**(11R):2139

[284] Nicolas Longiéras M, Sebban PP, Rivaton A, Gardette J-L. Degradation of epoxy resins under high energy electron beam irradiation: Radio-oxidation. Polymer Degradation and Stability. 2007;**92**(12):2190-2197

[285] Simos N, Zhong Z, Ghose S, Kirk HG, Trung L-P, McDonald KT, et al. Radiation damage and thermal shock response of carbon-fiber-reinforced materials to intense high-energy proton beams. Physical Review Accelerators and Beams. 2016; **19**:111002

[286] Memory JD, Fornes RE, Gilbert RD. Radiation effects on graphite fiber reinforced composites. Journal of Reinforced Plastics and Composites. 1988;**7**(1):33-65

[287] Abu Saleem RA, Abdelal N, Alsabbagh A, Al-Jarrah M, Al-Jawarneh F. Radiation shielding of fiber reinforced polymer composites incorporating lead nanoparticles—An empirical approach. Polymers. 2021;**13** (21):3699

[288] Dhand V, Mittal G, Rhee KY, Park S-J, Hui D. A short review on basalt

fiber reinforced polymer composites. Composites Part B: Engineering. 2015; **73**:166-180

[289] Arnhof M, Pilehvar S, Kjøniksen A-L, Cheibas I. Basalt fibre reinforced geopolymer made from lunar regolith simulant. In: Proceedings of the 8TH European Conference for Aeronautics and Space Sciences (EUCASS); Madrid, Spain: EUCASS; 2019

[290] Pilehvar S, Arnhof M, Erichsen A, Valentini L, Kjøniksen A-L. Investigation of severe lunar environmental conditions on the physical and mechanical properties of lunar regolith geopolymers. Journal of Materials Research and Technology. 2021;**11**:1506-1516

[291] Fiore V, Scalici T, Di Bella G, Valenza A. A review on basalt fibre and its composites. Composites Part B: Engineering. 2015;**74**:74-94

[292] Altun AA, Ertl F, Marechal M, Makaya A, Sgambati A, Schwentenwein M. Additive manufacturing of lunar regolith structures. Open Ceramics. 2021;**5**:100058

[293] Isachenkov M, Chugunov S, Akhatov I, Shishkovsky I. Regolith-based additive manufacturing for sustainable development of lunar infrastructure—An overview. Acta Astronautica. 2021;**180**:650-678

[294] Toutanji H, Schrayshuen B, Han M. New Glass Fiber Reinforced Concrete for Extraterrestrial Application. In: Earth & Space 2006: Engineering, Construction, and Operations in Challenging Environment. US: ASCE; 2006

[295] Rich B, Läkk H, Arnhof M, Cheibas I. Advanced concepts for ISRU-based additive manufacturing of planetary habitats. In: Conference Paper, 16th European Conference on Spacecraft Structures, Materials and Environmental Testing (ECSSMET 2021). Europe: ESA; 2021

[296] Mitchell A, Lafont U, Hołyńska M, Semprimoschnig CJAM. Additive manufacturing—A review of 4D printing and future applications. Additive Manufacturing. 2018;**24**: 606-626

[297] Arefin AME, Khatri NR, Kulkarni N, Egan PF. Polymer 3D printing review: Materials, process, and design strategies for medical applications. Polymers. 2021;**13**(9):1499